Available online at www.sciencedirect.com
ScienceDirect
Ore Geology Reviews 30 (2007) 1–29
ORE GEOLOGY REVIEWS
www.elsevier.com/locate/oregeorev

Copper, gold and silver enrichment in ore mylonites within massive sulphide orebodies at Hongtoushan VHMS deposit, N.E. China

Lianxing Gu [a,*], Yuanchuan Zheng [a], Xiaoqian Tang [a], Khin Zaw [a,b], Fernando Della-Pasque [a,b], Changzhi Wu [a], Zeman Tian [c], Jianjun Lu [a], Pei Ni [a], Xin Li [d], Futian Yang [d], Xiangwen Wang [d]

[a] *State Key Laboratory for Endogenic Metal Deposits Research (Nanjing University), Department of Earth Sciences, Nanjing University, Nanjing 210093, People's Republic of China*
[b] *CODES ARC Centre of Excellence in Ore Deposits, University of Tasmania, Private Bag 79 Hobart, Tasmania 7001, Australia*
[c] *Hongtoushan Copper Ltd., Fushun 113321, People's Republic of China*
[d] *Institute of Geology and Ore Exploration, Fushun 113321, People's Republic of China*

Received 1 November 2004; accepted 20 September 2005
Available online 2 February 2006

Abstract

The Hongtoushan Archaean Cu–Zn Volcanic-hosted Massive Sulphide (VHMS) deposit occurs in the Hunbei granite–greenstone terrane, Liaoning Province of NE China. The ores were metamorphosed (3.0–2.8 Ga) to upper amphibolite facies at temperatures between 600 and 650 °C, and underwent three phases of deformation. The deformation has transposed the stratiform orebodies into a Y-shaped configuration. Ore minerals in the deposit were originally composed of pyrite, pyrrhotite, chalcopyrite and sphalerite. Prograde metamorphism obliterated almost all the sedimentary textures in the ores, and the present ore textures were formed substantially during peak and post-peak metamorphism. Intensive remobilisations have occurred in the Hongtoushan deposit at various scales.

There are more than 30 oreshoots inside the main massive sulphide orebodies. The oreshoots range from 2 to 30 m in length, 0.1 to 1.5 m in width, and 2 to 30 m in depth extension. Most run parallel or sub-parallel to the strike of the massive sulphide ore layers with only a few being developed in metamorphic rocks in the immediate vicinity of the sulphide orebodies. Almost all the sulphide and gangue minerals in the oreshoots have been affected by intense shearing. Pyrite is characterised by cataclastic flow; pyrrhotite, chalcopyrite and sphalerite exhibit strong plasticity. Hydrothermal alteration minerals in the oreshoots are dominated by deformation-free hornblende, actinolite, epidote, clinozoisite, biotite, muscovite, albite, carbonate and quartz. Cu, Au and Ag in the ore mylonites average 11 wt.%, 1.74 and 235 g/t, respectively. Compared to the massive sulphide ores, these oreshoots show remarkable enrichment of these elements with enrichment coefficients of 5.3, 5.0 and 4.6, respectively. We draw the conclusion that these oreshoots are actually ore mylonites overprinted by late-stage fluids.

The presence of annealing textures in pyrrhotite and the absence in pyrite suggest that formation and succeeding annealing of the ore mylonite took place over the temperature range from 550 to 450 °C. Such a temperature range, combined with the geology and mineralogy, indicates that these ore mylonites and the derivative oreshoots were formed during upper-greenschist-facies retrograde metamorphism. Similarity of the ore mylonites to the massive ores in metal varieties and lead isotope ages suggest that Cu, Au and Ag of the overprinting fluids on the ore mylonites were derived mainly from the nearby massive sulphide ores.

* Corresponding author.
E-mail address: lxgu@nju.edu.cn (L.X. Gu).

0169-1368/$ - see front matter
doi:10.1016/j.oregeorev.2005.09.001

However, lead isotope compositions of the ore mylonites also suggest that an external source, such as the metamorphic host rocks, has also contributed to their metal budget.

Keywords: Ductile shear zone; Ore mylonite; Remobilisation; Massive sulphide deposit; Retrograde metamorphism; Hongtoushan; Liaoning

1. Introduction

Deformation and remobilisation of syngenetic massive sulphide deposits in volcanic and metamorphic terranes have yielded a large volume of literature (e.g., Vokes, 1969, 2000; McClay, 1983a; Vivallo and Rickard, 1990; Gu and McClay, 1992; Cook et al., 1993; Tiwary et al., 1998; Khin Zaw et al., 1997, 1999). In recent years, increasing attention has been paid to ductile response of the ores to deviatoric stress at high temperatures, which resulted in so-called 'durchbewegung' structures, piercement cusps and piercement veins (Marshall and Gilligan, 1989; Paakki et al., 1995), and ductile shear zones (McClay, 1983b; Duckworth and Rickard, 1993; Lydon et al., 2000) inside massive sulphide orebodies. Q.S. Zhang et al. (1984) and Liu et al. (1994) reported high enrichment of copper and gold in ore mylonites inside the massive sulphide orebodies at Hongtoushan, and explained that such enrichment in copper and gold was induced by differential mechanical remobilisation. However, documented accounts for highly metal-enriched ore mylonites within massive sulphide bodies are still scarce. This paper aims to describe ore mylonites inside massive sulphide orebodies at Hongtoushan, and discuss the mechanisms for high enrichment of copper, gold and silver in these mylonitised ores.

2. Regional geology

The Hongtoushan VHMS Cu–Zn massive sulphide deposit, Liaoning Province, occurs in the Hunbei Archaean terrane of northeastern China. The tectonic framework of NE China and the geology of the Hunbei terrane are described below.

2.1. Tectonic framework of NE China

Northeastern China consists of three major tectonic units (Fig. 1): the northern part of the North China Craton (NCC) in the south, the southern part of the Siberian Craton in the north, and the Central Asia Orogenic Belt (CAOB) positioned in between. The CAOB, in turn, comprises the Junggar–Xingan and the Tianshan–Tumen fold belts that are separated by the Junggar–Heggen suture (Z.M. Zhang et al., 1984; Deng, 1994; Shen et al., 1994b; Sun, 1992).

The NCC is the largest palaeo-continent in China (Yang et al., 1986; Ren, 1996; Zhai and Liu, 2003; Hart et al., 2002). The oldest metasedimentary rocks so far dated in western Liaoning Province have given an age as old as ~3.85 Ga on detrital zircons (Song et al., 1996). Early Archaean continental nuclei of this craton underwent multiple episodes of growth at 2.9 to 2.7, 2.6 to 2.4 and 1.9 to 1.8 Ga, resulting in a unified basement at some 1.8 Ga (Z.M. Zhang et al., 1984; Zhai and Liu, 2001; Zhao et al., 2001). During these episodes, rock units of the craton experienced extensive greenschist to granulite facies metamorphism, intensive migmatisation, and widespread magmatism (Z.M. Zhang et al., 1984; Chen et al., 1996, 1998; Zhai and Liu, 2003; Zhou et al., 2002).

The Central Asia Orogenic Belt (CAOB), extending westwards from northeastern China through southern Mongolia to the Altai Mountains, was developed by accretion of Palaeozoic island-arcs to the northern part of the North China and southern margins of the Siberian Craton (Fig. 1), with the formation of the Junggar–Xingan and Tianshan–Tumen fold belts, respectively (Li et al., 2004; Chen et al., 2000; Sengör et al., 1993; Hart et al., 2002). These accreted marginal fold belts collided along the Junggar–Heggen (also known as Solonker) suture (Tang, 1990; Sengör et al., 1993). This suture is defined by belts of highly deformed Permian marine sediments (Li et al., 2004), dismembered Palaeozoic ophiolites (Robinson et al., 1999), collision-related magmatic rocks (Chen et al., 2000), and local blueschists (Liou et al., 1989). However, complexity of terrane architectures makes it difficult to understand their evolution history and subduction polarity (Hart et al., 2002). Some authors (Robinson et al., 1999; Chen et al., 2000) suggest that convergence between the North China and Siberian Cratons was accompanied by north-dipping ocean subduction along the Juggar–Heggen suture, but others (Wang and Liu, 1991; Gu et al., 1999) argue that both the northern margin of the NCC and the southern margin of the Siberian Craton were active margins, and that accretion took place on both sides of the ocean. Furthermore, the timing of collision is still controversial. Although some authors argue that suturing took place

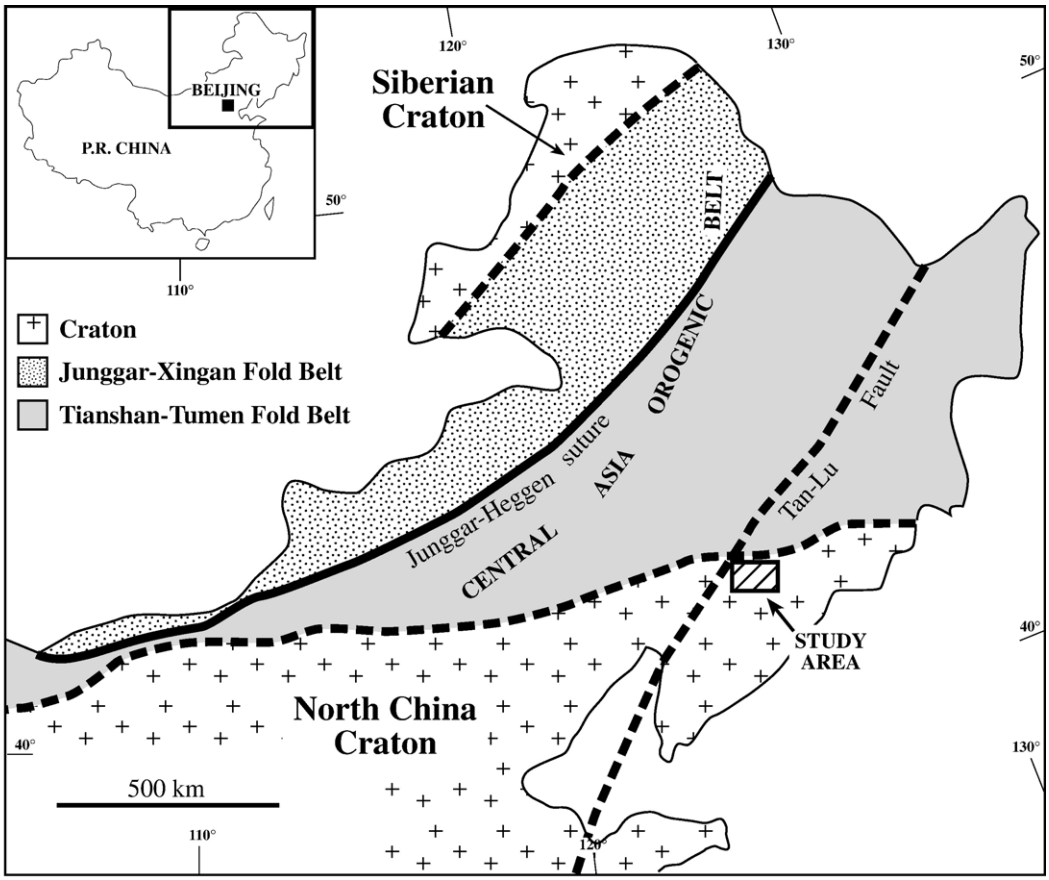

Fig. 1. Tectonic framework of northeastern China.

in either the Middle Devonian or Late Devonian to early Carboniferous (Hong et al., 1995), or in the Middle or Late Devonian (Tang, 1990; Xu and Chen, 1997), most authors propose that final amalgamation of these two continents took place in the Late Permian as a result of eastward diachronous collision (Wang and Liou, 1986; Sengör et al., 1993; Robinson et al., 1999; Chen et al., 2000).

Tectono-magmatism from Middle Jurassic to Cretaceous time, known as the Yanshanian movement in China (Z.M. Zhang et al., 1984; Yang et al., 1986), is believed to have been induced by the northwestward oblique subduction of the Izanagi–Pacific Plate beneath the eastern Asian continental margin (Tian et al., 1992; Yang et al., 2003; Xu, 2001). This event led to the formation of the NNE-trending Yanshanian magmatic belts and faulting in eastern China (Xu and Zhu, 1994, Hart et al., 2002). The Tan–Lu fault is a major tectonic feature of eastern China (Fig. 1). It can be traced for over 5000 km parallel to the present Asian continental margin with a sinistral displacement of about 700 km (Xu et al., 1987; Hart et al., 2002). A common consonance is that it was active in Late Jurassic to Early Tertiary times (Z.M. Zhang et al., 1984; Xu et al., 1987; Chen, 1989), although some geologists claim that the faulting could be traced back to Proterozoic and Palaeozoic time (Fitches et al., 1991; Fletcher et al., 1995). Some authors suggest that this fault was developed in response to the oblique subduction of the Izanagi–Pacific Plate since Jurassic time (Xu et al., 1987; Chen, 1989), but others believe (Zhu et al., 2004) that the large-scale displacement of this fault resulted from the continent–continent collision of the South and North China blocks in the Early Jurassic.

2.2. Geology of the Hunbei terrane

The Hunbei Archaean granite–greenstone terrane is located close to the intersection of the Tan–Lu fault with the northern boundary of the NCC (Fig. 1). This terrane is dominated by Early Archaean grey gneisses, mainly tonalitic, trondhjemitic and granodioritic in composition with minor supracrustal rocks metamorphosed to upper amphibolite facies. The grey gneisses

are overlain by several Early Archaean greenstone belts (Fig. 2). The grey gneisses and greenstones are exposed at a ratio of 3 : 2. The Hunhe and the Caoshi–Kaiyuan faults separate the Hunbei terrane from the Longgang terrane in the south and the Jingjiagou terrane in the northeast (Fig. 2). Both the Longgang and the Jingjiagou terranes are Archaean, but have a more restricted distribution of greenstones and show distinct structural discontinuity with the Hunbei terrane across the faults. The Longgang terrane is characterised by more intense migmatisation of the Archaean sequence (Zhao, 1981), and extensive Yanshanian magmatism and related mesothermal gold mineralisation, whereas the Jingjiagou terrane is distinctive for its granulite facies metamorphism and the occurrence of charnockite (Li et al., 1995; Chen et al., 1998). The greenstones of the Hunbei terrane are generally referred to as the Qingyuan Group, which comprises a vast sequence of gneisses and amphibolites. They have been further divided into the Jinfengling and Hongtoushan Formations (Fig. 3), which comprise the lower and the upper parts, respectively (Q.S. Zhang et al., 1984; Shen et al., 1994b). The Jinfengling Formation is dominated by amphibolites with intercalations of biotite gneisses and quartz–feldspar gneisses, while the Hongtoushan Formation contains more biotite gneisses and quartz–feldspar gneisses characterised in mineralogy by garnet, sillimanite and anthophyllite. Petrological and geochemical investigations by previous authors indicate that the parent volcanic rocks of the Qingyuan Group are continuously differentiated volcanic rocks varying in composition from mafic through intermediate to felsic of both the tholeiitic and calc-alkaline affinities, and are thus regarded as the likely products in an island-arc environment (Q.S. Zhang et al., 1984; Zhai et al., 1984; Li et al., 1995).

Q.S. Zhang et al. (1984) summarized previously reported isotope ages obtained by various methods and concluded that precursor rocks for the greenstones were older than 3.0 Ga, and were strongly metamorphosed to upper amphibolite facies during the period of 2.9 to 2.8 Ga. Later, Wang et al. (1987) reported an $^{40}Ar/^{39}Ar$ plateau age of 2.99 ± 0.1 Ga and an K–Ar age of 2.98 ± 0.04 Ga for hornblende from amphibolite of the Jingfengling Formation. These two ages are fairly consistent within errors, and thus an age of 2.99 Ma was taken by these authors as the formation age of the amphibolite. Li et al. (1995) obtained a whole-rock Sm–Nd isochron age of 2.84 ± 0.05 Ma for the amphibolite from the Jingfengling Formation as well. These ages of Wang et al. and Li et al. are roughly consistent with the conclusion of Q.S. Zhang et al. (1984) and indicate that

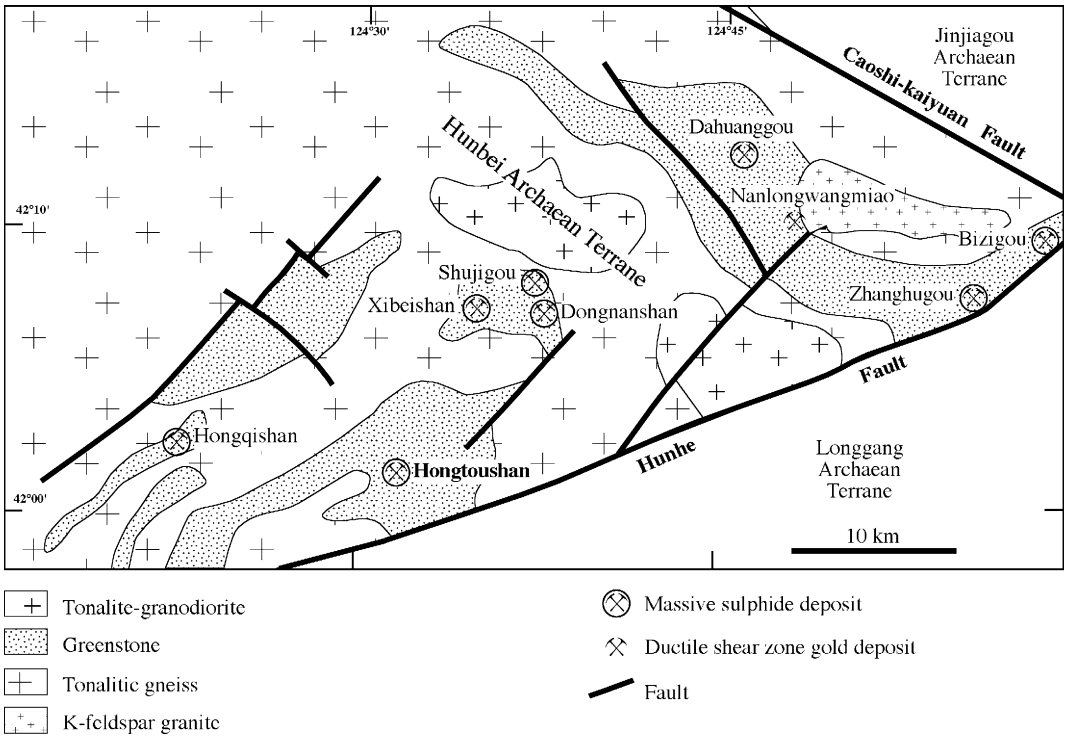

Fig. 2. Geology of the Hunbei granite–greenstone terrane.

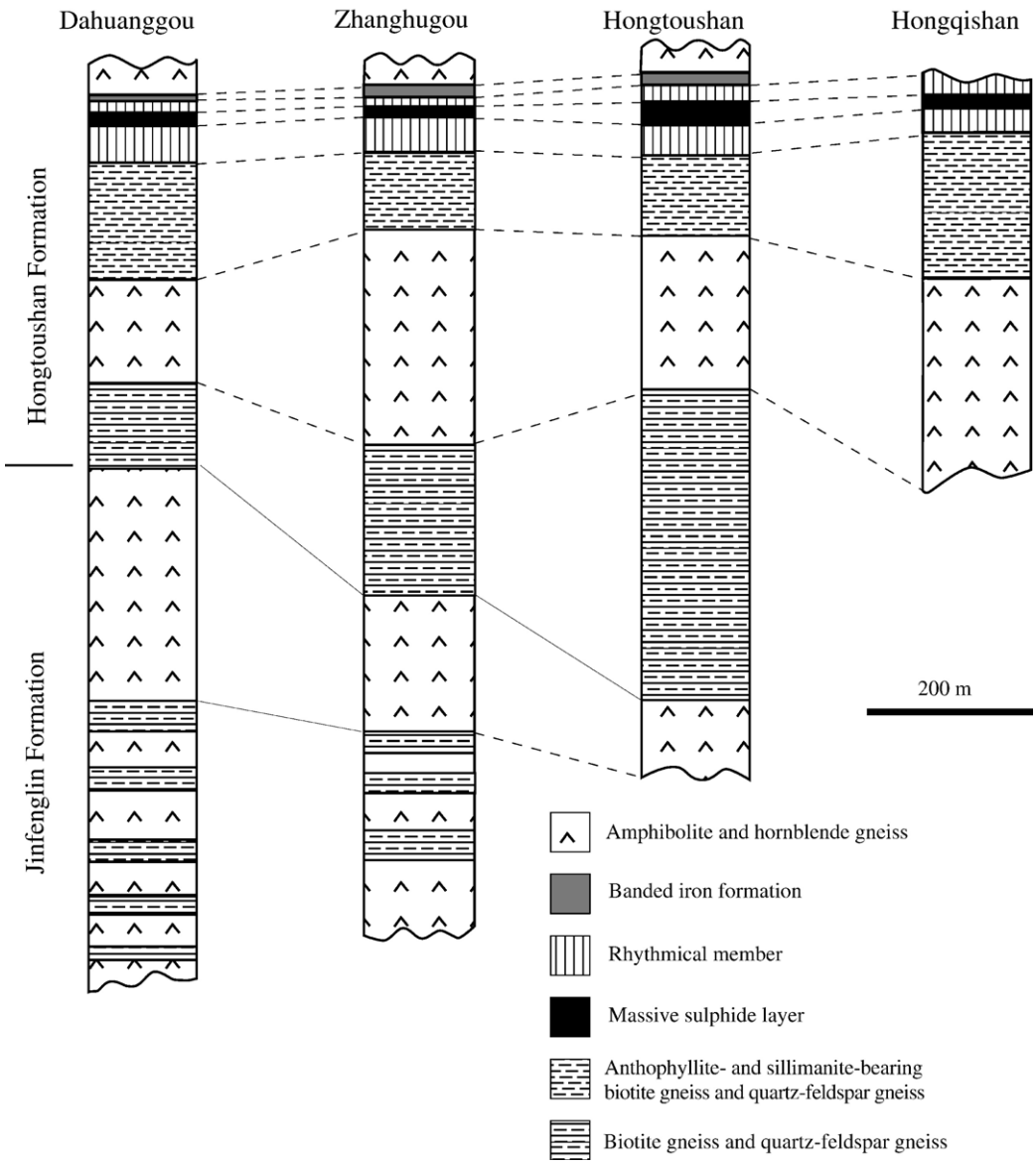

Fig. 3. Stratigraphic positions of the main massive sulphide deposits in the Hunbei terranes.

metamorphism of the precursor rocks for the greenstones took place in the time interval of 3.0–2.8 Ma. Post-orogenic granites are represented by the medium- to coarse-grained gneissose Shujigou tonalite (Fig. 2), which was dated at 2551 ± 0.001 Ma and 2578 ± 0.001 Ma by zircon U–Pb (Shen et al., 1994a) and $^{40}Ar/^{39}Ar$ plateau (Wang et al., 1986) methods, respectively. In the absence of age data, it was commonly assumed that the Hongshilazi K-feldspar granite to the east of Nanlongwangmiao (Fig. 2) was formed around 2.5 Ga (Q.S. Zhang et al., 1984; Li et al., 1995). However, we recently obtained a zircon U–Pb age of 159.6 ± 2.8 Ma for this granite by the LA-ICP-MS method (manuscript in preparation), indicating that it is a Mesozoic granite comparable in age to many granites in the coastal areas of eastern China.

2.3. Mineralization in the Hunbei terrane

Mineralization in the Hunbei terrane belongs to two types: volcanic-hosted massive sulphides and ductile shear zone gold. More than 100 massive sulphide deposits and smaller occurrences have been found within the Hunbei greenstone belts. Eight of them (Hongtoushan, Hongqishan, Bizigou, Zhanghugou, Xibeishan, Dongnanshan, Shujigou and Dahuanggou; Fig. 2) have been

mined for Cu, Zn and S, but all of these mines except those at Hongtoushan and Hongqishan have been shut down due to exhaustion of the ore. Metal tonnages, grades and mining status of these eight deposits are briefly listed in Table 1.

The Archaean submarine exhalative origin of the massive sulphide deposits of the Hunbei region and their characteristics have been well documented by previous authors (e.g., Q.S. Zhang et al., 1984; Liu et al., 1994; Deng, 1994; Shen et al., 1994a; Hou et al., 1999). All these deposits are confined to a stratigraphic interval of about 100 m in thickness (Fig. 3). This interval, termed the rhythmical member by local geologists, belongs to the upper portion of the Hongtoushan Formation and is composed of rhythmic interbeds of mica gneisses, quartz–feldspar gneisses, hornblende gneisses and amphibolites that are overlain by Banded Iron Formation (BIF) (Fig. 3) composed predominantly of magnetite and quartz. Compositionally, these rhythmic layers are characterised by the presence of garnet, anthophyllite and sillimanite. Based on petrological and geochemical studies, Zhai et al. (1984) and Deng (1994) interpreted that these rocks were derived from precursors composed of basaltic–andesitic–dacitic lavas and tuffaceous rocks intercalated with sands, silts, and clays.

The Nanlongwangmiao gold deposit is the only ductile shear zone deposit in the Hunbei terrane. This shear zone occurs in the greenstones of the Hongtoushan Formation and extends parallel to the strike of the greenstones in the northwest direction. It is about 5 km in length and 0.5 to 1 km in width. A gold-mineralised section, 1500 m long and 35 to 95 m wide, in this shear zone is composed of 46 lenticular or stratiform orebodies. Individual orebodies are 1 to 3 m in width with maximum surface extension up to 200 m along strike and depth extension up to 300 m (Li et al., 1995). The total gold reserve of the deposit is estimated at 4 t, with an average grade of 4 g/t. Gold occurs either in association with disseminated-veinlet pyrite and pyrrhotite in the mylonitised gneisses, or in pyrite-bearing quartz lodes, and mostly as native gold with average fineness of 946 (Liu et al., 1994). The gold-bearing ductile shear zone is cut by pegmatite veins. A Rb–Sr isochron age of 2.41 Ga has been obtained for muscovite from one of the veins by Fushun Geological Research Institute (quoted from Liu et al., 1994; Li et al., 1995). Mining of this deposit has not yet been started.

3. Geology of the Hongtoushan deposit

The Hongtoushan deposit is the largest of the eight Archaean volcanic-hosted massive sulphide Cu–Zn deposits in the Hunbei district. Surface mining was done by local residents early in the 1930s, and large-scale underground operation began in the 1960s after systematic drilling. Further drilling during mining has

Table 1
Metal tonnages and grades of main massive sulphide deposits in the Hunbei terrane

Deposit	Metal tonnage	Grade	Mining status
Hongtoushan	0.5 Mt Cu	1.5–1.8 wt.% Cu	About 1/3 of the ores have been mined
	0.7 Mt Zn	2.0–2.5 wt.% Zn	
	20 t Au	0.5–0.8 g/t Au	
	1000 t Ag	20–60 g/t Ag	
Hongqishan	0.013 Mt Cu	2.88 wt.% Cu	More than 90% of the ores have been mined
	0.027 Mt Zn	6.18 wt.% Zn	
	0.088 Mt S	17.02 wt.% S	
		5 g/t Ag	
Bizigou	0.007 Mt Cu	0.9 wt.% Cu	Mine shut down
	0.026 Mt Zn	3.19 wt.% Zn	
	0.08 Mt S	13.32 wt.% S	
Zhanghugou	0.00226 Mt Cu	1–2 wt.% Cu	Mine shut down
	0.09 Mt Zn	12 wt.% Zn	
Xibeishan	0.016 Mt Cu	1.17 wt.% Cu	Mine shut down
	0.021 Mt Zn	1.85 wt.% Zn	
Dongnanshan	0.008 Mt Cu	1.13 wt.% Cu	Mine shut down
	0.013 Mt Zn	1.82 wt.% Zn	
Shujigou	0.033 Mt Cu	1.3 wt.% Cu	Mine shut down
	0.092 Mt Zn	2.0 wt.% Zn	
Dahuanggou	0.003 Mt Cu	2.23 wt.% Cu	Mine shut down
	0.038 Mt Zn	2.51 wt.% Zn	
	10 Mt<S	19.05 wt.% S	

identified new orebodies. According to the latest report, the deposit has a metal reserve of 0.5 Mt Cu at 1.5% to 1.80% Cu, 0.7 Mt Zn at 2.0% to 2.5% Zn, 20 t Au at 0.5 to 0.8 g/t Au and 1000 t Ag at 20 to 60 g/t Ag. Average concentrations of S, Se and Cd are 20% to 22%, 25 and 56 g/t, respectively. At the end of 2004, about one third of the ore had been mined.

The main orebodies, although intensely deformed, are stratiform and were stratigraphically controlled by the 'rhythmic member' in the upper part of the Hongtoushan Formation (Fig. 3). Q.S. Zhang et al. (1984) divided this unit into five sub-members, each of which is composed of several layers of different lithology. These sub-members, from the inferred bottom to the top, are: (1) biotite gneiss and quartz–feldspar gneiss with amphibolite intercalations (20 m thick), (2) amphibolite intercalated with biotite gneiss, hornblende gneiss and quartz–feldspar gneiss (20 m thick), (3) interbedded hornblende gneiss, biotite gneiss and quartz–feldspar gneiss (25 m thick), (4) biotite gneiss and quartz–feldspar gneiss characterised by garnet, sillimanite and anthophyllite (25 m thick), and (5) quartz–feldspar gneiss with intercalations of hornblende and biotite gneiss (12 m thick). The individual layers within each of the sub-members range from dm to 5 m in thickness. Massive sulphide orebodies occur in the upper part of the fourth sub-member of this rhythmic interval.

The host rocks of the massive sulphide ores have been metamorphosed to upper amphibolite facies. Based on the biotite–garnet geothermometer, Zhao and Cui (1987) obtained a peak metamorphic temperature between 600 and 650 °C. Foliations of the rocks are roughly parallel to lithological boundaries and dip towards SE at angles between 60 and 80°, resulting in a vertically plunging fold (Fig. 4). Yang and Yu (1984) distinguished three phases of deformation (D_1 to D_3) that occurred between 2.8 and 2.5 Ga in the mine area. D_1 is characterised by formation of axial foliations (S_1) and small-size tight folds (F_1), which plunge to the north at 20 to 30°. D_2 resulted in medium- to large-scale, steeply dipping or vertically plunging folds with associated ductile faulting. The present NEE-trending lineations (Fig. 4) were mainly formed during this phase. D_3 is a less intensive phase resulting in broad, approximately N–S-trending and vertical or slightly inclined folds.

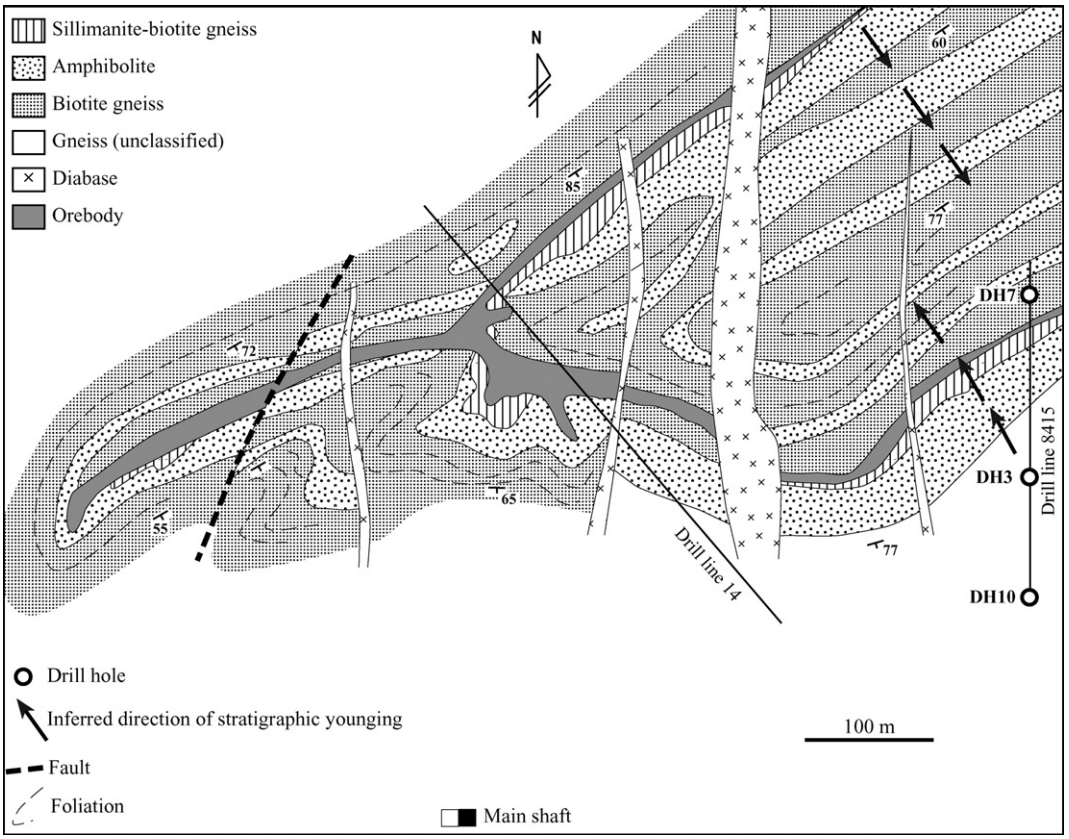

Fig. 4. Geology of the Hongtoushan deposit at Level −167 m.

In harmony with foliations of the surrounding rocks, the massive sulphide layers dip generally towards the southeast (Fig. 4), forming a vertically plunging synformal fold (Yang and Yu, 1984). Mining operations have reached a depth of 1337 m. The orebodies at all levels above −467 m exhibit a Y-shaped form, with the two arms opening toward east (Figs. 4 and 5). These two arms merge into a single entity and then continue toward the west. Y-shaped deformation structures are also commonly seen in the gneissic wall rocks of the mine area. Such similarity in deformation patterns of the ore layers to the confining metamorphic rocks points towards a pre-deformation age for the sulphide ores.

The vertical hinge of the synformal fold is located at the junction of three arms of the Y-shaped orebody (Figs. 4 and 5), where the orebodies reach their maximum thickness and thus form a large vertical 'ore pillar', as it is informally called by mining geologists. The 'ore pillar' varies between 70 and 100 m in length and 20 and 40 m in width at different levels. It extends almost vertically from the surface (+430 m) down to −907 m, but as the dip of the synform hinge changes gradually northeastwards, the 'ore pillar' also changes in dip angle to 45° at a depth of 1017 m to 10° at a depth of 1257 m below surface. According to Yang and Yu (1984), the 'ore pillar' was formed by syn-kynematic plastic flow of the sulphide mass that accompanied the D_2 event. Piercement cusps have also been reported in the marginal parts of the massive sulphide orebodies (Q.S. Zhang et al., 1984; Deng, 1994).

Most of the ores are massive, but banded structures comprising alternating and synchronously folded sulphide and gneiss layers also occur locally. Although no stringer or brecciated zone has been identified as a conduit for submarine hydrothermal exhalations, zones of disseminated mineralisation occur in metamorphic rocks adjacent to the main orebodies. These zones, tens of meters thick and more than 100 m in length, have Cu and Zn contents below the economic grade, but locally contain exploitable ore pods.

Sulphide minerals amount to 60 to 80 vol.% of the massive sulphide ores. Ore minerals are dominated by pyrite, pyrrhotite, sphalerite and chalcopyrite in approximate proportions of 5 : 5 : 1 : 1. Less abundant are cubanite, electrum, chalcocite and magnetite; galena is only locally seen. Gangue minerals are dominated by quartz with lesser plagioclase, garnet, hornblende, actinolite, biotite, muscovite and gahnite. Zn/Cu values generally increase with depth. Ores with higher Cu grades (2.51 to 3.50 wt.%) are at mine levels above 0 m, whereas those with higher Zn grades (2.51 to 3.50 wt.%) are found below the 0 m level (Lu, 1994). $\delta^{34}S$ of sulphide minerals (Deng, 1994) varies from −1.2‰ to +5.6‰ (CDT).

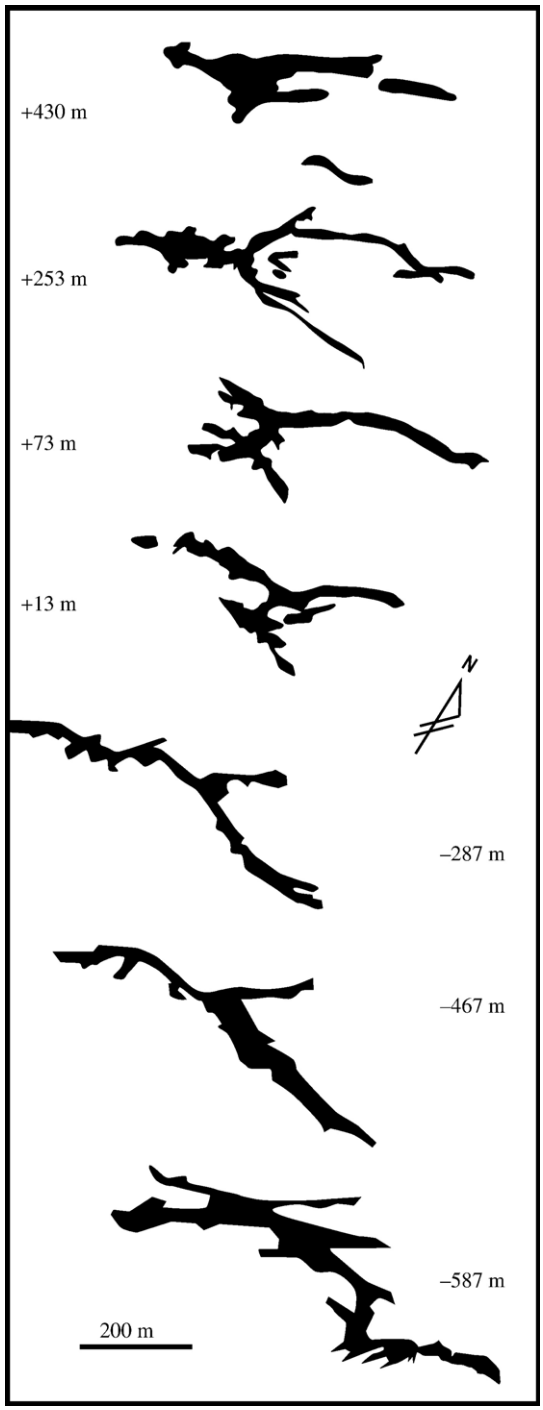

Fig. 5. Orebody arrays of the Hongtoushan deposit at levels above −587 m.

Sulphide-bearing veins and vugs are ubiquitous throughout the deposit. The veins are millimeters to

decimeters in width and cut the massive sulphide ores in variable directions with sharp and relatively straight boundaries. In some places, the massive sulphide ores close to the veins are intensely silicified. Branching and thickness variation along strike, and mutual crosscutting of the veins, are also common. However, no veins have been found cutting the mylonitic ores. The vugs, either irregular or lenticular in shape, are normally centimeters to decimeters in size. Most of the veins and vugs contain pyrite, pyrrhotite, chalcopyrite and sphalerite as dominant sulphides; quartz is the dominant gangue with minor carbonates. This mineralogy is basically consistent with the overall composition of the massive sulphide ores. However, one vein that carries a significant amount of galena is also present. Most of the veins and vugs are not folded, and the minerals are free of deformation, although veins cut by exposure-scale faults can also be seen.

No granite intrusions have been found in the mine area. However, numerous diabase dykes cut the massive sulphide orebodies and the host metamorphic rocks with sharp contacts. Varying from decimeters to more than 50 m in width, most of them extend consistently in approximately N–S directions (Fig. 4), with local branching. Xenoliths of the ores and metamorphic rocks, centimeters to decimeters in size, can be found inside the dykes. The rocks contain variable amounts of pyroxene, plagioclase and hornblende with minor magnetite and pyrite. The occurrence of 1 to 2 vol.% quartz indicates that these rocks are tholeiitic in composition. The diabase is normally fresh without conspicuous hydrothermal alteration and sulphide mineralisation, but in some localities sulphide-bearing quartz veins, millimeters or centimeters in width, are seen cutting the dykes. Carbonate and chlorite alteration of the diabase can be discerned in the immediate vicinity of these veins. Free of deformation textures, these dykes were thought to have been emplaced under post-kinematic environments (Q.S. Zhang et al., 1984). Recently, we obtained a LA-ICP-MS zircon U–Pb age of 2534 ± 0.011 Ma for the thickest diabase dyke in Fig. 4 (manuscript in preparation).

4. Sampling and analytical methods

A total of 285 samples of ores, quartz veins, diabase and metamorphic rocks were collected both at the surface and from 8 underground mining levels (between Level −370 and −744 m). Thin sections, polished sections and polished blocks were made from the rock and ore samples. For the purpose of discrimination of pyrrhotite structures, the polished sections were coated with the magnetic colloid prepared after the description of Craig and Vaughan (1981). Polished blocks were etched by nitric acid (1 : 4) for 15 min to observe the grain boundaries and twins of sphalerite.

Microscopic identification of anhydrite and gahnite was verified on a Renishaw RM2000 Raman microprobe at the State Key Laboratory for Endogenic Metal Deposits Research, Nanjing University. Excitation was achieved using an argon laser at a wavelength of 514 nm with laser power of 5 mW, slit width of 50 μm, collecting time of 20 s and scanning range of 1600–100 cm^{-1}.

Samples for geochemical analyses were ground to pass 200 mesh, and further ground and homogenised in an agate mortar under alcohol. Gold, Ag, Cu, Pb and Zn contents were determined by atomic absorption on a WFX-1E2 spectrometer at the Laboratory of Geoexploration Company No. 814. A deuterium lamp for background correction and an air–acetylene mixture for fuel were used.

Lead isotope determinations were performed on a Thermal Ionisation Mass Spectrometer Triton TI at State Key Laboratory for Endogenic Mineral Deposits Research, Nanjing University. Samples were washed in distilled water, and digested in a mixture of double distilled concentrated HNO_3 and HCl (at 2 : 1). Pb was separated and purified by HBr and anion exchange resin (BioRad AG1X8, 200 to 400 mesh) and then coated on a rhenium strip by classic H_3PO_4 and silicon gel method. Mass fractionation corrections of Pb isotopic compositions for the samples were made relative to International Standard NIST Pb-981, which was determined at the same temperature (1250 °C) as the samples. The NIST Pb-981 gives mean $^{206}Pb/^{204}Pb$, $^{207}Pb/^{204}Pb$, and $^{208}Pb/^{204}Pb$ ratios of 16.8839 ± 0.0008, 15.4207 ± 0.0016, and 36.4753 ± 0.0029, respectively during the period of sample analysis. Precisions of analyses for Pb isotope ratios are estimated to be better than 0.05%. Lead isotope ages were calculated based on the two-stage model proposed by Stacey and Kramers (1975).

5. Mineralogy and texture of massive sulphide ores

Massive sulphide ores at Hongtoushan are characterised by porphyroblastic textures with pyrite porphyroblasts in matrices composed of variable amounts of pyrrhotite, pyrite, chalcopyrite, and sphalerite (Fig. 6A, B). On the basis of matrix mineralogy, the ores can be divided into pyrrhotite-and sphalerite-types. The matrix of the pyrrhotite-type ore is dominated by pyrrhotite with lesser chalcopyrite and sphalerite (Fig. 6A, B), and

minor cubanite, electrum, chalcocite and magnetite, whereas sphalerite is the prevailing sulphide in the matrix of the sphalerite-type ore. These two ore types normally have gradational boundaries, although the sphalerite-type ore increases in amount with depth. Galena is absent or present in minor amounts in both types. Characteristics of the main components of the massive sulphide ores are described below.

5.1. Gangue minerals

Gangue minerals of the massive sulphide ores are dominated by quartz, plagioclase, hornblende, biotite, garnet, sillimanite and gahnite, with lesser epidote, clinozoisite and carbonate. More than 90% of the gangue minerals in the massive sulphide ores form globular textures. The globules, with either smooth or curved boundaries, vary in dimension mostly from 2 to 5 mm — occasionally up to more than 10 mm, and are commonly included in pyrite porphyroblasts (Fig. 6A, B). Mineralogically, the globules can be divided into felsic mineral and dark mineral globules.

Felsic mineral globules consist of either a single grain or aggregated grains of quartz in most cases (Fig. 6C), and occasionally plagioclase, and hence show light grey colour in hand specimen. Such globules are commonly surrounded by selvages composed of tiny hydrous minerals including hornblende, biotite, muscovite and epidote. Quartz grains in globules are most commonly free of deformation. How-

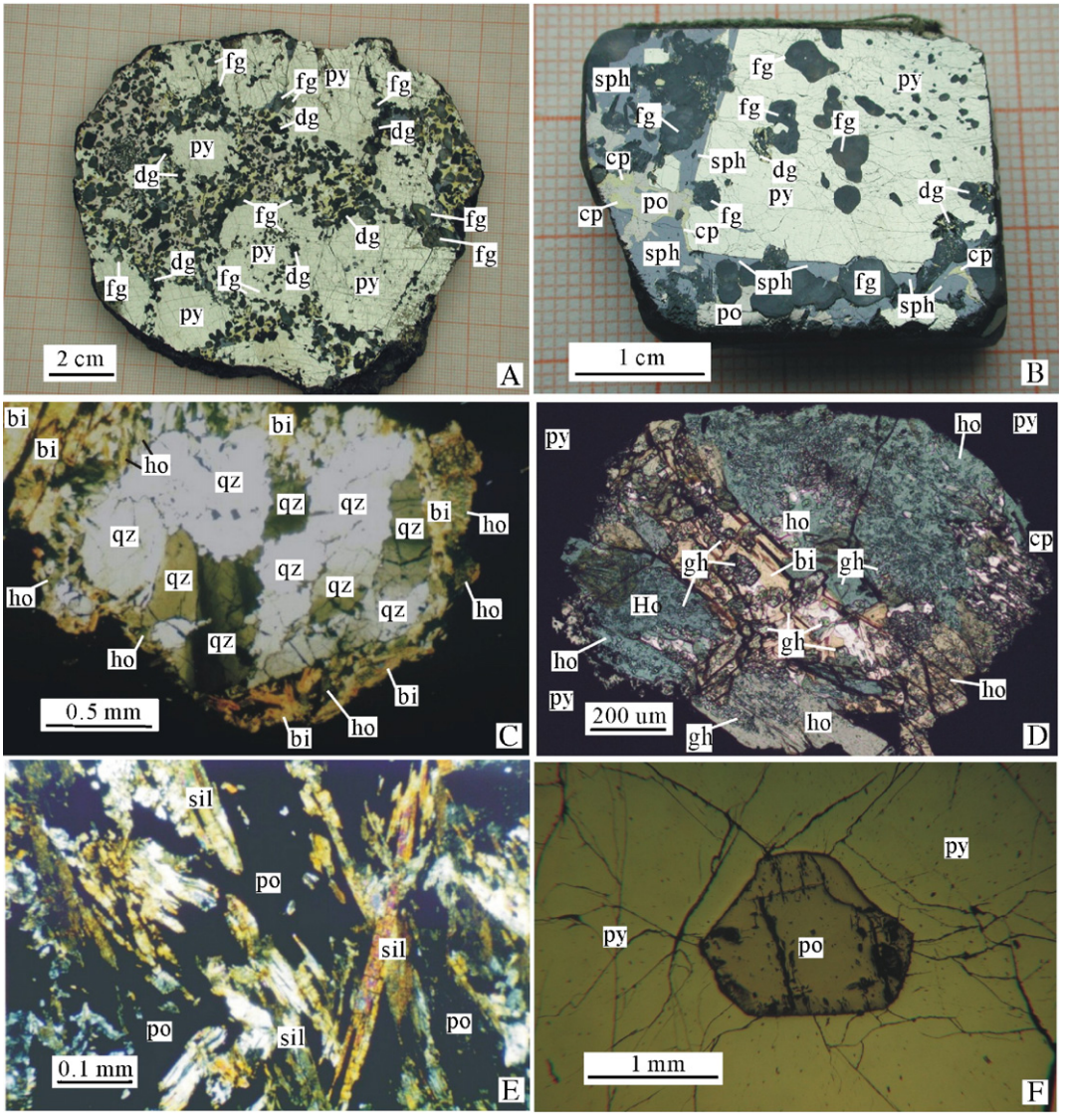

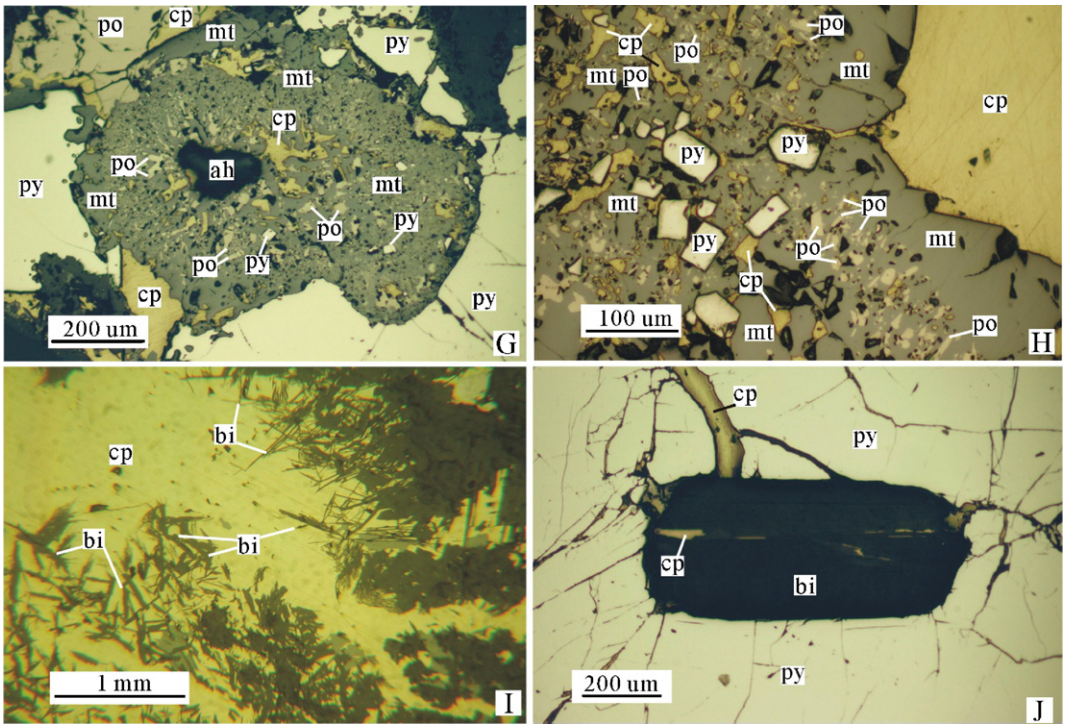

Fig. 6. Textures of massive sulphide ores from Hongtoushan. Mineral abbreviations: ah — anhydrite; bi — biotite; cp — chalcopyrite; dg — dark mineral globule; fg — felsic mineral globule; gh — gahnite; ho — hornblende; ms — muscovite; mt — magnetite; po — pyrrhotite; py — pyrite; qz — quartz; sil — sillimanite; sph — sphalerite. A) Pyrite porphyroblasts in massive sulphide ore. Crystal boundaries of porphyroblasts are pinned by both felsic mineral and dark mineral globules, but the boundaries between two pyrite crystals are straight (polished surface). B) A pyrite porphyroblast in massive sulphide. Crystal boundaries of the porphyroblast are pinned by both felsic mineral and dark mineral globules, but the boundaries of this porphyroblast against pyrrhotite, sphalerite and chalcopyrite are straight (polished surface). C) Globule composed of dynamically recrystallised quartz enveloped by a rim of mica and hornblende (transmitted light with crossed nicols). D) Dark globule included in a pyrite porphyroblast with tiny grains and aggregates of gahnite included in hornblende and biotite (transmitted light). E) Annealed pyrrhotite separated by sillimanite (transmitted light with crossed nicols). F) Pyrrhotite crystal included in a pyrite porphyroblast (plane reflected light). G) A core of anhydrite surrounded by a shell of magnetite aggregates in intergrowth with fine-grained pyrrhotite plates and pyrite cubes. The magnetite in the shell margin lacks intergrown pyrrhotite and corrodes pyrite, pyrrhotite and chalcopyrite surrounding the shell (plane reflected light). H) Magnetite in the margin of a shell and core structure replaces chalcopyrite with intergrown pyrrhotite and cubic pyrite. Intergrown pyrrhotite is absent in the magnetite adjacent to the boundary between the magnetite and the replaced chalcopyrite (plane reflected light). I) Acicular biotite flakes replacing chalcopyrite (plane reflected light). J) A biotite crystal with remobilised chalcopyrite along its cleavage is included in a pyrite porphyroblast (plane reflected light).

ever, there are also deformed grains that show dynamic recrystallization with seriated new grain boundaries (Fig. 6C). In some localities, static equilibrium of recrystallisation resulted in new grains with 120° dihedral angles and grain sizes generally >0.2 mm. As a less fluid-resistant mineral, plagioclase is characterised by much wider hydrous-mineral selvages than quartz, and in some cases only occur as relics surrounded by hydrous minerals. Maximum extinction angles of the plagioclase indicate that it is dominantly andesine ($An_{30–40}$). Pyrite, pyrrhotite, chalcopyrite and sphalerite grains and aggregates are included in some of the felsic mineral globules.

Dark mineral globules (Fig. 6A, B, D) are dark green in hand specimen and are dominated by hornblende and biotite with less garnet and gahnite, and minor muscovite, quartz, plagioclase and sillimanite. Hornblende in the globules is greenish blue under the microscope, and mostly 0.1 to 0.5 mm in grain size, and occasionally exceeds 1 mm. Biotite and muscovite form, respectively, light brown and colourless flakes 0.1 to 0.5 in length. This is in contrast with the biotite outside the globules, which is usually over 1 mm in flake length and commonly replaced by chlorite. Garnet forms colourless euhedral and isotropic grains mostly 0.2 to 0.5 mm, but in some cases as large as 1 mm in size. Gahnite grains, a few micrometers to 100 μm in size, occur as disseminated or aggregated light green subhedral or euhedral crystals with high relief and rhombic or triangular cross-sections (Fig. 6D). This mineral occupies

10–25 vol.% of the dark mineral globules and is commonly included in hornblende, biotite and garnet (Fig. 6D). It gives the highest peaks at 661.21 and 416.21 cm^{-1} in the Raman spectrum. Quartz is developed as anhedral grains. Sillimanite occurs as relics replaced by biotite. There are two generations of plagioclase. The first generation is represented by andesine occurring as partly replaced relics, whereas the second features anhedral to subhedral grains with lower anorthite content ($An_{<15}$). Replacement relics of sulphide minerals such as pyrrhotite, pyrite, sphalerite and chalcopyrite are also found in the dark mineral globules. Unlike those included in the felsic mineral globules, these sulphides normally show embayed or irregular boundaries. In contrast to quartz in the felsic mineral globules, silicate minerals inside the dark mineral globules are normally free of deformation textures.

5.2. Pyrrhotite

Pyrrhotite comprises 20% to 80% of the ore minerals by volume. It occurs in the matrix between pyrite porphyroblasts, and has a grain size of 2 to 5 mm, occasionally up to 10 mm. Most of the pyrrhotite has straight grain boundaries due to recrystallisation or incipient annealing, while local triple-junction or foam textures indicate annealing equilibrium (Stanton, 1972; Vokes and Craig, 1993). The development of elongated, oriented and strain-free grains may have resulted from recrystallisation and growth in kinked matrices (Stanton, 1972). Most of the pyrrhotite grains are free of deformation textures, but deformation twins, kink bands and subgrains can occasionally be observed. Annealed pyrrhotite can be separated by sillimanite prisms, sometimes into optically continuous islands (Fig. 6E). Pyrrhotite grains with either straight or curved boundaries are found included in pyrite porphyroblasts (Fig. 6F). Inclusions of pyrrhotite in quartz and plagioclase globules are also common. In contrast, no inclusions or reaction relics of pyrite occur inside pyrrhotite grains. Coating with magnetic colloid reveals that the pyrrhotite is almost purely hexagonal (Gu et al., 2001).

Secondary pyrrhotite is also present in the massive sulphide ores. It can be seen replacing pyrite porphyroblasts with curved or sinuous boundaries, or occurs as fissure-filling veins in the ores. This generation is characterised by intergrowth of the hexagonal variety with abundant monoclinic exsolution lamella, similar to that reported by Gu and Vokes (1996) for some Norwegian deposits. Like pyrite, pyrrhotite also precipitated as symplectites with replacive magnetite (Fig. 6G, H).

5.3. Chalcopyrite

Chalcopyrite is the most important Cu-bearing mineral at Hongtoushan and makes up 5 to 10 vol.% of the pyrrhotite-type massive sulphide ores. It forms patches of aggregates in the matrix to pyrite porphyroblasts and is also commonly present as inclusions in pyrite porphyroblasts and gangue mineral globules, implying that it was a primary mineral of submarine exhalation.

Patches of chalcopyrite aggregates are commonly replaced by acicular biotite, 0.2 to 0.5 mm in length (Fig. 6I). The biotite that replaces chalcopyrite is much smaller in size than that included in pyrite porphyroblasts (Fig. 6J). Chalcopyrite is also replaced by magnetite, resulting in worm-like secondary chalcopyrite in symplectitic intergrowth with the replacive magnetite (Fig. 6G, H). At sites where chalcopyrite coexists with pyrite, pyrrhotite and sphalerite, chalcopyrite always shows preferential replacement by silicates and magnetite.

Chalcopyrite is the most common mineral filling partially cleavage-controlled fractures in pyrite porphyroblasts or tensional pull-apart fractures in deformed pyrite. Some of the fracture walls fit together if the infilling chalcopyrite is removed, but others have been embayed and do not match. Chalcopyrite also corrodes the outer rims or edges of pyrite porphyroblasts, resulting in embayed boundaries. Precipitation of remobilised chalcopyrite along cleavages of coarse-grained biotite is a common phenomenon. Such biotite is often bent or kinked, and is hence comparable in nature to the prograde-metamorphic biotite included in porphyroblastic pyrite.

5.4. Sphalerite

Sphalerite occupies 5 to 10 vol.% of the pyrrhotite-type massive ores and can amount to more than 20 vol.% in the sphalerite-type ores. Widely developed inclusions of sphalerite in pyrite porphyroblasts and gangue mineral globules indicate that this mineral was also a primary phase prior to prograde metamorphism. Sphalerite in both ore-types is black and occurs mostly as aggregates in the matrix to pyrite. Etching (1 : 1 HNO_3) reveals grain sizes varying between 0.1 and 0.5 mm. Most of the grains are characterised by relatively straight boundaries with regular and straight growth twins, indicating recrystallisation. Sphalerite also fills fractures of pyrite and cleavages of biotite, but the amount is insignificant relative to chalcopyrite.

Unlike sphalerite of many other massive sulphide deposits (e.g., Barton, 1978; Eldridge et al., 1983; Craig and Vokes, 1993; Gu et al., 1998), most of the sphalerite grains from Hongtoushan are poor in micrometer-sized chalcopyrite blebs (chalcopyrite disease; Barton, 1978). However, heavy chalcopyrite disease can also be found where late-stage chalcopyrite replaced or veined the sphalerite, which agrees well with the observation of Vokes and Craig (1993). Sphalerite replaced by biotite and actinolite is also seen in some samples.

5.5. Pyrite

Three modes of occurrence of pyrite can be distinguished in the massive sulphide ores. Pyrite of the first mode is typified by monomineralic grains or aggregates with other sulphides included in gangue mineral globules. The second mode is represented by pyrite porphyroblasts, whereas pyrite of the third mode occurs as replacement products in association with magnetite (see Section 5.6).

Pyrite porphyroblasts occupy 5 to 20 vol. % in most samples, and reach more than 50 vol.% in some localities. They vary in grain size from 5 to 30 mm, and in some cases up to 50 mm. Although most of their boundaries against the gangue mineral globules are ragged, boundaries against other pyrite porphyroblasts or grains of other sulphides, such as pyrrhotite, chalcopyrite and sphalerite are straight and have 90° dihedral angles (Fig. 6A, B), indicating that these porphyroblasts are cubic. Inclusions in the porphyroblasts include pyrrhotite, chalcopyrite, sphalerite and gangue mineral globules (Fig. 6A, B, D). Biotite is the most common euhedral gangue mineral included in pyrite porphyroblasts (Fig. 6J) and occurs mostly as euhedral plates >0.5 mm in grain size (Fig. 6J). This is in contrast to the acicular or anhedral minute flakes <0.5 mm in length that replace chalcopyrite (Fig. 6I) or occur in the dark mineral globules (Fig. 6D). Deformation textures of porphyroblastic pyrite are weak and dominated by cataclastic fractures. The fractures are commonly filled by remobilised chalcopyrite with lesser pyrrhotite and sphalerite.

Another generation of pyrite is formed by late-stage retrograde hydrothermal alteration. This generation of pyrite is characterised by small (<0.5 mm) cubes in association with magnetite that replaced pre-existing sulphides (Fig. 6G, H).

5.6. Magnetite

Magnetite occurs in the massive sulphide ores as shells around a core of gangue minerals (Fig. 6G). Such core and shell structures, mostly 1.5 to 2.5 mm in size, are spherical, ovoid, lens-like or flat in shape. The shells, mostly 0.2 to 0.5 mm in width, are composed of intergrowths of tiny plates of pyrrhotite with magnetite aggregates (Fig. 6G, H), and sometimes are disseminated with fine cubes of pyrite (Fig. 6H). Pyr-

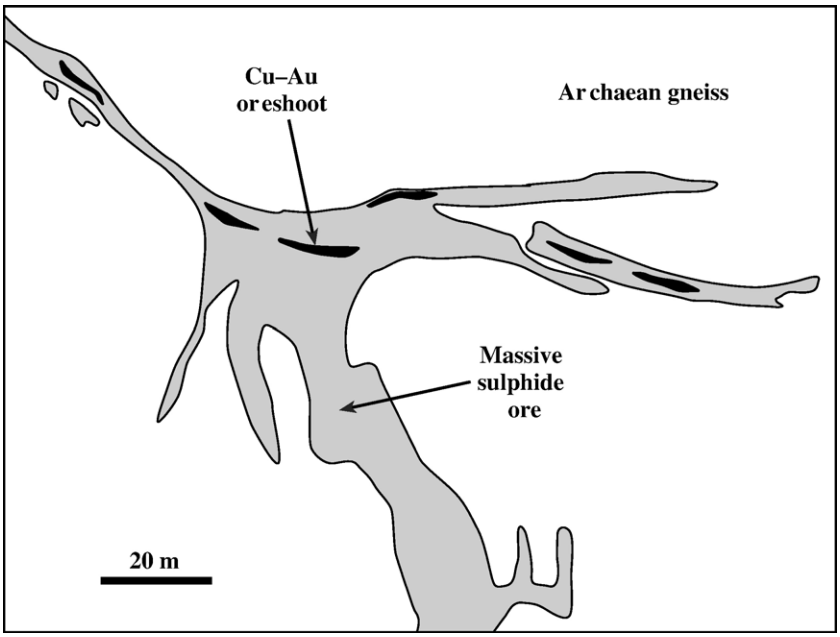

Fig. 7. Distribution of oreshoots at level −227 m of the Hongtoushan deposit.

rhotite, chalcopyrite and even porphyroblastic pyrite outside the shells are commonly corroded and are sometimes cut by magnetite (Fig. 6G, H). In the case of pyrrhotite, an original grain can be cut into several isolated, but optically continuous, islands. These textures indicate that magnetite of the shells were formed at the expense of the pre-existing sulphides.

The tiny pyrrhotite plates are randomly oriented in all the shells, and in the case where the replaced mineral is also pyrrhotite (Fig. 6G), they do not show continuous extinction with the remnant pyrrhotite. This indicates that they are not relics of the replaced pyrrhotite, but instead a new phase formed by replacement reaction. It is interesting to note that the magnetite shells usually have a margin that lacks intergrown pyrrhotite (Fig. 6G, H). Like the pyrrhotite plates, the fine pyrite cubes seems to have been formed by the sulphur released during replacement of magnetite on surrounding sulphide minerals.

The cores, 0.5 to 1.5 mm in size, have sinuous boundaries with the magnetite shells (Fig. 6G). They are mostly composed of a single crystal of carbonate or anhydrite, and occasionally include one or more euhedra of amphibole. The carbonate shows perfect rhombohedral cleavages and polysynthetic twins with very high birefringence, while the anhydrite, with polysynthetic twins and cleavages in three directions at right angles, shows interference colour ranging up to the third order and gives a peak at 1017.8 cm^{-1} in the Raman spectrum.

5.7. Electrum

Gold and silver in massive sulphide ores occur mainly as electrum grains 1 to 20 μm in size. Microprobe analyses of five grains give Au contents in the range 52.34 to 70.28 wt.% with a mean of 61.47 wt.% (Liu et al., 1994). Most of the electrum occurs as inclusions in chalcopyrite, pyrite and pyrrhotite, as well as in gangue minerals.

5.8. Galena

Galena is found only under the microscope in a few samples, and forms anhedral grains <0.5 mm in size. Megascopic galena up to 1 cm in size occurs in a quartz-sulphide vein cutting the massive sulphide ore. In addition to pyrite and chalcopyrite, galena is also a major constituent of this vein, although sphalerite is not present. Straight cleavage and curved grain boundaries imply that neither conspicuous deformation nor annealing has affected the galena in this vein.

6. Mylonite-type oreshoots

6.1. Distribution

There are at least 30 mylonite-type oreshoots. These oreshoots are mostly found inside the main massive sulphide ore-layers, but some are along the contact with the wall rock gneisses (Fig. 7), and only a few are in the metamorphic rocks in the immediate vicinity of the orebodies. These oreshoots range from 2 to 30 m in length, 0.1 to 1.5 m in width and 2 to 30 m in depth extension, and hence are much larger in size than the sheared pods at Renström, northern Sweden (Duckworth and Rickard, 1993). They are responsible for less than 10% of the total ore reserves, however, and are of minor economic importance relative to the massive ores in the deposit. Most of the oreshoots run parallel or sub-parallel to the strike of the massive sulphide ore layers (Fig. 7), commonly showing sharp boundaries against metamorphic rocks, but are gradational towards the nearby massive ores (Fig. 8).

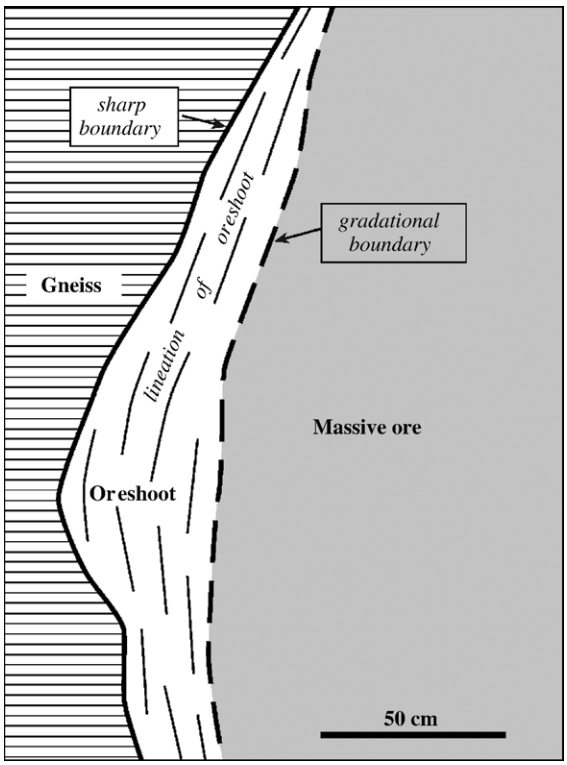

Fig. 8. Sketch showing sharp and gradational contacts of an oreshoot with gneiss and massive sulphide ore, respectively, on level −647 of the Hongtoushan mine.

6.2. Deformation texture

The oreshoots appear gneissose on the underground mining exposures with steep lineations approximately parallel to the dip of the host massive sulphide orebodies and to the wallrock gneissosity where the oreshoots occur close to the metamorphic rocks. At hand specimen scale, the lineations are defined predominantly by the intensely plastically deformed minerals, such as pyrrhotite, sphalerite and quartz, and their aggregates (Fig. 9A, B), and to a lesser extent by pull-apart fragments of brittle minerals such as pyrite, silicates and

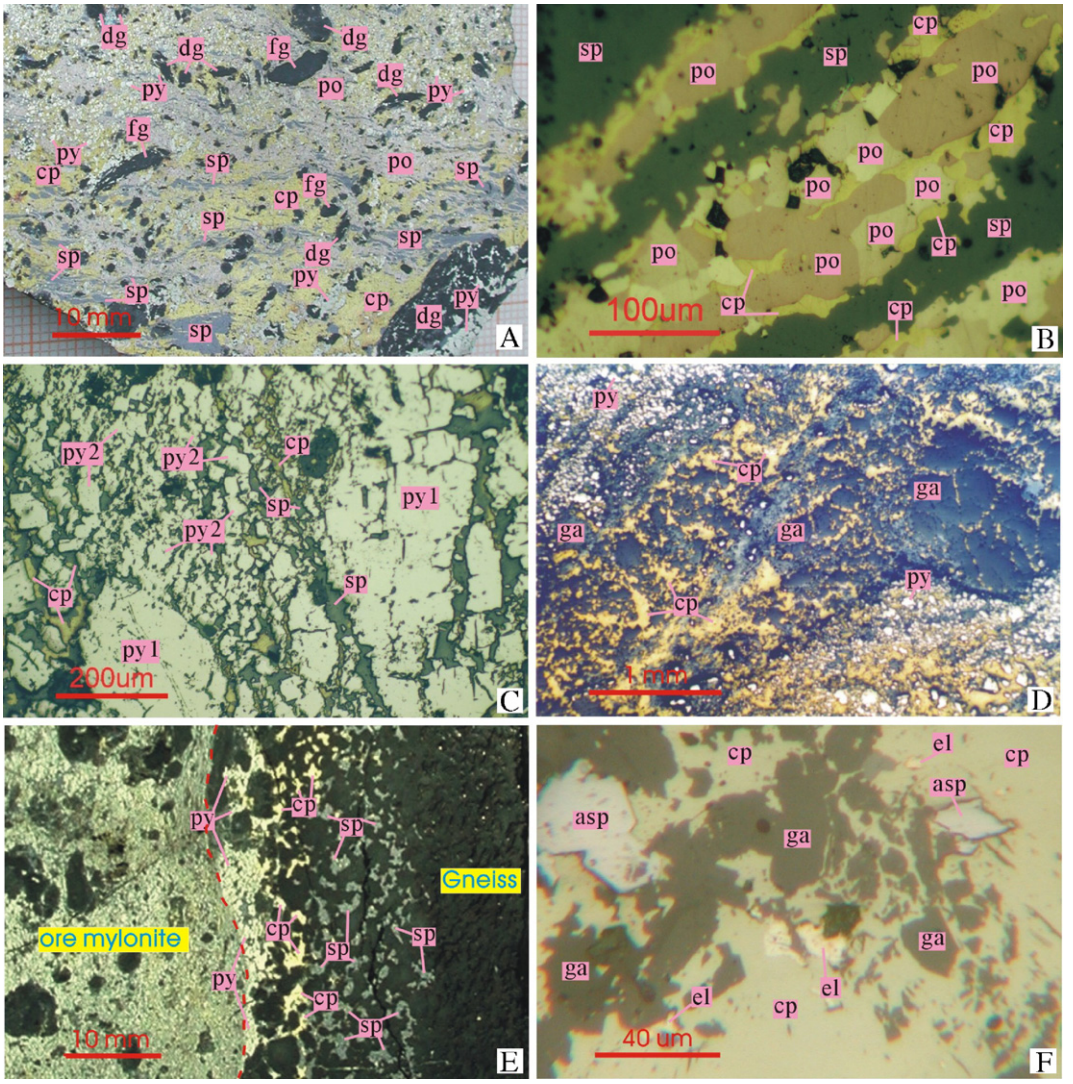

Fig. 9. Structures and textures of the ore mylonites from the Hongtoushan deposit. Abbreviations as in Fig. 6. A) Ore mylonite with ductile shear foliation. Pyrite has been crushed into minute fragments <1 mm in size. Pyrrhotite, chalcopyrite and sphalerite have been plastically deformed and show shear foliation. Felsic mineral and dark mineral globules are stretched, pulled apart and possibly rotated (polished surface). B) Foliated ore mylonite with alternating sphalerite and pyrrhotite+chalcopyrite layers. Triple junction textures of pyrrhotite indicate annealing equilibrium has been attained (reflected light with slightly oblique nicols). C) Two generations of pyrite in the ore mylonite. Lense-like shape of py1 indicates pressure solution. Some cracks of the cataclastically deformed pyrite (py1) have been healed by remobilised pyrite (py2). Py2 also occurs in the matrix as cubic or irregular grains in intergrowth with chalcopyrite and sphalerite (plane reflected light). D) Remobilised chalcopyrite occurring as anastomosing veins cutting deformed quartz. Pyrite in the upper left part of the picture has been cataclastically deformed, and the fragments have been rounded and two-dimensionally displaced, such that the original grain is difficult to reassemble (plane reflected light). E) Contact between an ore mylonite and its wall gneiss (marked by a red broken line). Mineralisation zoning, outwards from the contact to the gneiss, is shown by a transition from pyrite through chalcopyrite to sphalerite (polished surface). F) Electrum-bearing sample of the ore mylonite, where electrum (el) occurs as undeformed rectangular crystals in a matrix of chalcopyrite. Arsenopyrite (asp) occurs as rhombic euhedra partly corroded by chalcopyrite and gangue minerals (ga).

magnetite (Fig. 9A, B). The long axes of some of the elongated globular aggregates are not parallel to the foliation, suggesting that the globules have been rotated. Minerals in the samples include those inherited from the massive ores, such as pyrite, pyrrhotite, chalcopyrite, sphalerite, magnetite, quartz, plagioclase, hornblende, biotite, garnet and epidote, and those formed by late-stage fluid precipitation, including pyrite, chalcopyrite, pyrrhotite, sphalerite, arsenopyrite, electrum, quartz, albite, hornblende, actinolite, biotite, epidote and carbonates. Deformation textures can be divided into the cataclastic and plastic categories.

6.2.1. Cataclastic deformation texture

Minerals dominated by cataclastic deformation are plagioclase, hornblende, epidote, pyrite and magnetite. Plagioclase is essentially cataclastically deformed, although deformation lamellae of the fragments are also common. The fragments, varying in size and displacement, have sharp and rounded edges. Some nearly rhombic-shaped fragments are offset and aligned along shear directions (Fig. 10A). Hornblende and epidote have been pulled apart along cleavages into tiny fragments, which are also aligned along shear directions.

Pyrite is characterised by cataclastic deformation and porphyroclastic textures. The fragments are mostly <0.2 mm in size, in sharp contrast to the millimeter- or centimeter-sized pyrite crystals in the undeformed ores. Initial shearing of a pyrite metablast in the massive sulphide ores resulted in rhombohedral or nearly rectangular pull-apart fragments cut by a set of microfractures (Fig. 10B). Further shearing has fragmented single pyrite grains, which are now separated by more plastic minerals such as chalcopyrite and pyrrhotite, and aligned along shear directions (Fig. 10B). The morphology of the original pyrite grain can be reassembled from the fragments in the case of limited and unidirectional displacement. However, two-dimensional displacement accompanying rolling movement will make the fragments rounded and scattered in two dimensions, such that reassembly of the original grain will be hampered and the fragments could sometimes be mistaken for original small grains (Fig. 10C). Some pyrite cataclasts show concentric fractures and are surrounded by a zone of peeled-off tiny fragments, indicating that rotation of the pyrite grains occurred locally (Vokes, 1969; Marshall and Gilligan, 1989).

Magnetite also shows intense cataclastic deformation and has been sheared into minute fragments aligned along shear directions, indicating that formation of this mineral predates shearing of the massive ores.

6.2.2. Plastic deformation texture

Minerals dominated by plastic deformation are quartz, biotite, chalcopyrite, pyrrhotite and sphalerite. Quartz globules of the original massive ores have been sheared into lineated ribbons or flamboyants, which have been dynamically recrystallised (Fig. 10D) or annealed to equilibrium. Most of the new grains resulting from annealing equilibrium are characterised by small grain size (between 0.05 and 0.2 mm). Curved flakes, undulose extinction and kink bands of micas are commonly seen. Some flakes have been sheared into typical "mica fish" (Fig. 10A; Sun et al., 1998; Grotenhuis et al., 2003). Dark mineral globules of the massive ores have been commonly elongated (Fig. 9A). In these globules, quartz and micas also show plastic deformation. Grain boundary sliding of the component silicates might have occurred as well.

As the principal matrix-forming minerals, pyrrhotite, chalcopyrite and sphalerite behaved plastically in the ores from the oreshoots. Intense stretching of the grains resulted in alternating layers of these minerals (Fig. 9A, B), although cases also occur where sphalerite is sheared into flat and lineated lenses in a matrix of more plastic chalcopyrite or pyrrhotite. Post-shear annealing is typically indicated by strain-free pyrrhotite grains with straight to gently curved boundaries. Foam textures of this mineral are also commonly seen (Fig. 9B). Recrystallised pyrrhotite grains, a few to tens of micrometers in size, are significantly smaller than those in the undeformed massive sulphide ores. The pyrrhotite is almost purely hexagonal and lacks lamellar intergrowths of the monoclinic variety. By contrast, no evidence has been found for recrystallisation of pyrite.

Although pyrite from the oreshoots is dominated by brittle deformation, weak plastic flow is manifested by dislocation and pressure solution textures. In polished sections etched by ammonium dichromate, abundant pits can be seen on the surface of pyrite porphyroclasts (Fig. 10E). These pits, typically aligned in one or two crystallographic directions of the host, are 1 to 2 μm in width and up to hundreds of micrometers in length, and can either be straight or gently curved. They represent slip lines that were formed where a glide plane intersects the observed surfaces (Clark and Kelly, 1973) and are characterised by high dislocation densities resulting from repeated passage of dislocations along the same glide planes (Cox, 1987; Gu and McClay, 1992). In some pyrite fragments, dislocation tangles revealed by branching or knitted slip lines can be seen, indicating dislocation–dislocation interactions at high strain (Cox, 1987). In other fragments, picket-fence arrays of slip lines (Fig. 10E) are indicative of dislocation walls

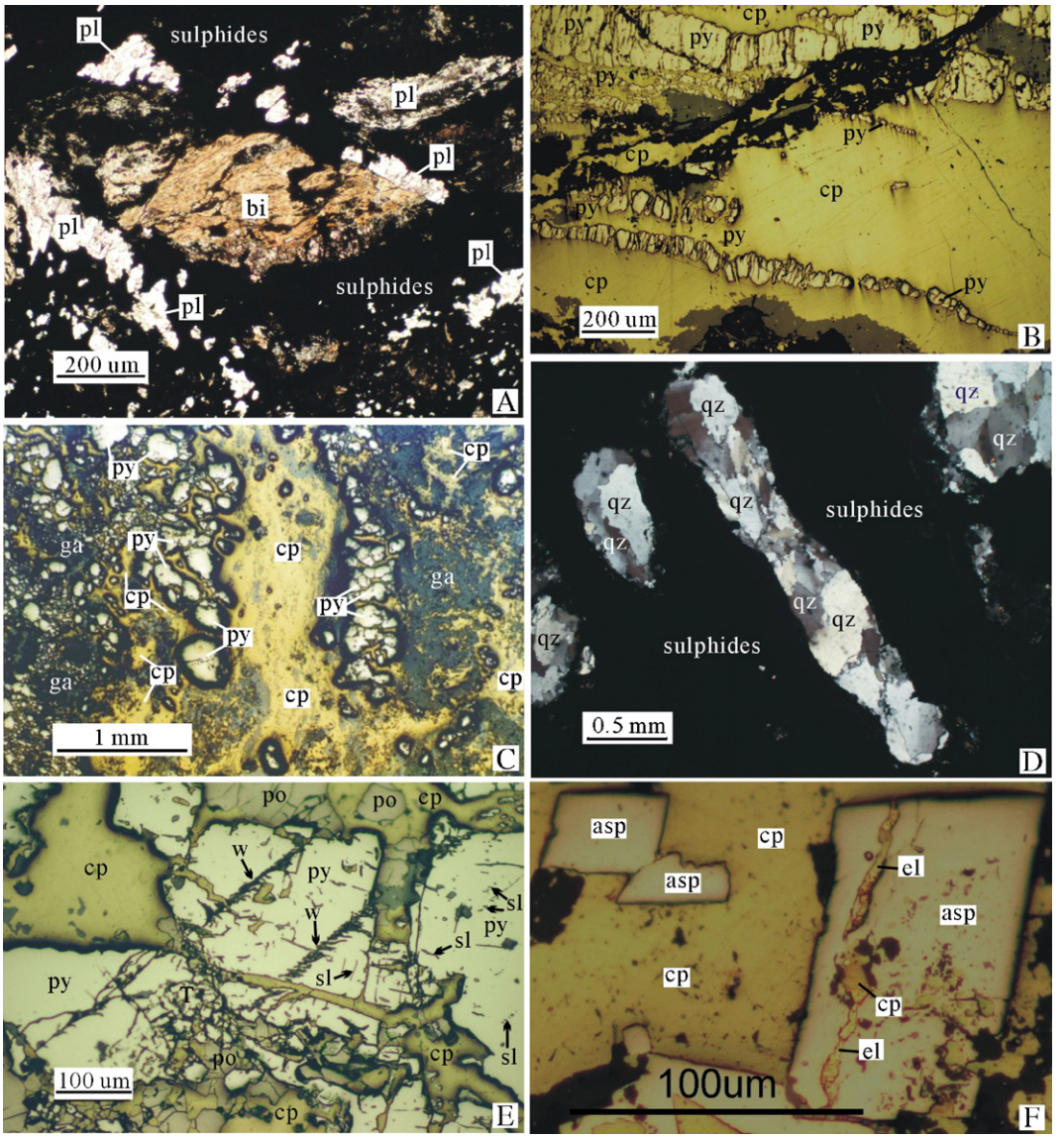

Fig. 10. Microphotographs for textures of the ore mylonites from the Hongtoushan deposit. Mineral symbols as in Fig. 6. A) Cataclastically deformed plagioclase and a mica fish in ore mylonite (transmitted light). B) Intensely sheared and cataclastically deformed pyrite crystals in a plastic chalcopyrite matrix. Rhombic or nearly rectangular pull-apart fragments of the pyrite are aligned along shear direction (plane reflected light). C) Pyrite porphyroclasts of varying restorability in the ore mylonite. An original pyrite grain can be restored from fragments on the right half of the picture. However, it is difficult to restore the original grains from the fragments on the left half of the picture due to two-dimensional displacement and possible rotation of the fragments. Note that silicate gangues (ga) are intensely replaced by chalcopyrite (plane reflected light). D) An intensely stretched and dynamically recrystallised quartz ribbon in an ore mylonite sample (transmitted light). E) Pyrite porphyroclasts cut and corroded by chalcopyrite with embayed boundaries, indicating precipitation of the chalcopyrite from a fluid. Slip lines (sl) revealed by alignment of dislocation etch pits can be seen on the surfaces of pyrite. In the fragment central to the picture, picket-fence arrays of slip lines represent dislocation walls (W). Two parallel walls run northeastward through the entire fragment (polished section etched by ammonium dichromate; plane reflected light). F) Electrum (el) together with chalcopyrite filling a crack of a rhombus arsenopyrite (asp) crystal (plane reflected light).

formed by both gliding and climbing of edge dislocations (Cox, 1987). Straight and heavily etched dislocation walls running through the entire fragments (Fig. 10E) could develop into fractures with further deformation. In some samples of the ore mylonite, deformed pyrite show lens-shaped outlines (Fig. 9C), indicating that pressure solution might have accompanied shearing (McClay and Ellis, 1983; Cox, 1987).

6.3. Remobilisation texture

Although ore mylonites are usually dominated by deformed minerals inherited from the parental massive sulphide ore assemblage, the textures also indicate that significant amounts of pyrite, chalcopyrite, arsenopyrite, electrum and other minerals were introduced by late-stage remobilisation fluids. Beside the cataclastically deformed grains (py1 in Fig. 9C), there is a second generation of pyrite (py2 in Fig. 9C) in the ore mylonites. This generation, mostly 5 to 20 μm in size, usually displays well-polished and clear surfaces, and is more resistant to oxidation in air than the cataclastic pyrite, indicating a poorly deformed lattice and a post-kinematic origin. This generation of pyrite occurs mainly as: (1) irregular grains; (2) vermicular rods intergrown with chalcopyrite and to a lesser extent with sphalerite; and (3) microscopic veins up to tens of micrometer cross-cutting chalcopyrite and pyrrhotite. The vermicular intergrowth of pyrite with chalcopyrite is likely to have been formed by co-precipitation from fluids. Fractures of cataclastically deformed pyrite healed by pyrite are also commonly seen (Fig. 9C). It follows that this generation was deposited by late-stage fluids.

Chalcopyrite, and in fewer cases sphalerite and pyrrhotite, commonly fill cracks of pyrite porphyroclasts in the ore mylonite. Embayed walls of some infilling veins (Fig. 10E) indicate that replacement corrosion has affected the host pyrite and that these sulphides were introduced and deposited, accompanying the opening of cracks in the brittle pyrite. Well-developed chalcopyrite disease (Barton, 1978) can be found in sphalerite where this mineral is cut by chalcopyrite veinlets. Sulphides, particularly chalcopyrite, are also ubiquitously seen filling cracks, fissures and cleavages of plagioclase, mafic silicates and lithoclasts. Silicate minerals, due to their chemical instability, were more intensely replaced by sulphides than was pyrite (Fig. 10C). Although quartz is characterised by limited replacement, chalcopyrite does replace quartz in irregular or anastomosing veins (Fig. 9D). This could imply that chalcopyrite was precipitated from infiltrating fluids through fissures that were diminutive due to the highly plastic behaviour of quartz in response to high-temperature and water-present deformation (Spry, 1979).

A sample collected from a stope on Level −707 m in the mine shows the sharp contact between an ore mylonite zone and the adjacent gneiss (Fig. 9E). The ore mylonite in this sample contains abundant tiny fluid-precipitated pyrite grains. Away from the contact, sulphide mineralisation in the gneiss exhibits clear zoning from pyrite through chalcopyrite to sphalerite. Such a zoning is no doubt produced by sequential precipitation of the sulphides from a fluid that percolated into the gneiss from the ore mylonite.

Arsenopyrite is commonly seen in the ore mylonites but not in the massive sulphide ores. It typically occurs in a matrix of chalcopyrite as columnar euhedra with rhombic cross-sections (Fig. 9F, 10F), and in some cases, forms aggregates of more than twenty crystals. The grains vary in size between 0.01 and 0.05 mm and occasionally up to 0.1 mm. Most of them are typically deformation-free, although a few grains are cut by fissures filled with chalcopyrite and electrum (Fig. 10F). Some of the arsenopyrite crystals have been replaced by chalcopyrite or silicates along their margins, resulting in embayed boundaries (Fig. 9F, 10F). These textures indicate that arsenopyrite was precipitated later than ductile shearing of the massive ores.

Electrum has been identified in a single polished section from the ore mylonite (HT-90, Table 1). This sample contains more than ten rectangular or irregular grains of 1 to 30 μm in size. Most of the grains are included in chalcopyrite (Fig. 9F), with a few growing on the surface of arsenopyrite. In some cases, this mineral is a constituent of the sealing materials in the fissures cutting arsenopyrite (Fig. 10F). The rectangular shape of some of the grains (Fig. 9F) suggests post-shear precipitation of the electrum, while the fissure-filling occurrence is likely to indicate that electrum was introduced by fluids subsequent to the crystallisation of arsenopyrite. Microprobe analysis of five electrum grains yielded Au and Ag contents (wt.%) of 15 and 85, 21 and 79, 29 and 71, 28 and 72, and 37 and 63, respectively, indicating low fineness of these grains.

Various types of hydrothermal alteration are extensively developed in the oreshoots. Alteration minerals are dominated by hornblende, actinolite, epidote, clinozoisite, biotite, muscovite, albite, carbonate and quartz. These alteration minerals are deformation-free, and can occur either as replacive patches or in veinlets cutting deformed minerals. Such alteration assemblage and the greenish blue pleochroism of the replacive hornblende are likely to indicate an upper greenschist facies environment (Miyashiro, 1994).

7. Metal contents and isotopes

7.1. Metal contents

Six samples of the massive sulphide ores have Cu, Au and Ag contents averaging 2.08 wt.%, 0.35 g/t and 51.33 g/t, respectively, while these elements in five ore mylonite samples average 11.00 wt. %, 1.74 g/t and

Table 2
Analyses of ore metals for two different ore types

Ore type	Sample no	Sample location (level, stope)	Cu (wt.%)	Au (g/t)	Ag (g/t)	Pb (wt.%)	Zn (wt.%)	Ag/Au
Massive sulphide ore	HT-50	−467 m, 1#	1.82	0.23	54	0.017	0.79	234.8
	HT-66	−587 m, 2 #	1.49	0.07	38	0.019	2.20	542.9
	HT-68	−587 m, 4 #	2.17	0.64	50	0.023	1.48	78.1
	HT-77	−647 m, 3#	2.10	0.20	50	0.015	2.54	250.0
	HT-85	−707 m, 3 #	0.86	0.58	22	0.014	2.21	37.9
	HT-216	−467 m, 3#	4.06	0.36	94	0.032	2.84	261.1
	average		2.08	0.35	51.33	0.020	2.01	146.7
Ore mylonite	HT-5	−467 m, 1 #	16.43	1.23	337	0.0048	1.01	274.0
	HT-9	−527 m, 1#	7.65	0.69	164	0.016	1.30	237.7
	HT-16	−647 m, 9–10#	15.84	0.97	278	0.0037	3.46	286.6
	HT-90	−707 m, 7 #	12.58	2.65	303	0.044	2.86	114.3
	HT-91	−707 m, 7 #	2.52	3.15	94	0.025	9.61	29.8
	average		11.00	1.74	235.2	0.019	3.65	135.2
Enrichment coefficient			5.3	5.0	4.6	0.9	1.8	

Enrichment coefficient = average concentration of ore mylonite vs. massive sulphide ore.
Relative errors obtained by repeated determinations for varying metal ranges are 66.6% for 0.05 to 0.5 g/t Au, 50% for 0.5 to 1 g/t Au, 30% for 1 to 2 g/t Au, 20% 2 to 5 g/t Au, 20% for 10 to 50 g/t Ag, 15% for 50 to 100 g/t Ag, 10% for 0.5 to 3 wt.% Cu, 7 % for >3 wt.% Cu, 30% for 0.003 to 0.01 wt.% Pb, 25% for 0.01 to 0.1 wt.% Pb, 20% for 0.4 to 1.0 wt.% Zn, and 15% for 1.0 to 10 wt.% Zn.

235.2 g/t, respectively (Table 2). Compared to the pre-shearing massive sulphide ores, Cu, Au and Ag have enrichment coefficients in the ore mylonites of 5.3, 5.0 and 4.6, respectively. In contrast, no conspicuous enrichment of Pb and Zn has been found in the ore mylonite relative to the massive sulphide ores. Microscopically, almost all the sphalerite in ore mylonite sample HT-91 has been affected by shearing, indicating that the Zn content of 9.61 wt.% in this sample was inherited from the pre-shearing massive sulphide ore. Enrichment of Cu, Au and Ag in the ore mylonite is basically consistent with the mine records where mylonitic ore grades (averaging 15.20 wt.% Cu, 1.54 g/t Au and 231.4 g/t Ag), are much higher than the massive sulphide ores (averaging 3.69 wt.% Cu, 0.46 g/t Au and 59.96 g/t Ag).

7.2. Lead isotope geochemistry

Lead isotope analyses (Table 3) indicate that massive sulphide ores from Hongtoushan are characterised by a restricted range of radiogenic leads, i.e., $^{206}Pb/^{204}Pb$ = 13.58 to 13.65, $^{207}Pb/^{204}Pb$ = 14.52 to 14.63, and $^{208}Pb/^{204}Pb$ = 33.42 to 33.74. Plots of the samples on $^{207}Pb/^{204}Pb$–$^{206}Pb/^{204}Pb$ and $^{208}Pb/^{204}Pb$–$^{206}Pb/^{204}Pb$ diagrams (Fig. 11) show a linear array with limited

Table 3
Lead isotope analyses of the ores and the wall rocks from Hongtoushan with calculation results of Stacey and Kramers two-stage model ages

Ore type	Sample	$^{206}Pb/^{204}Pb$	2σ	$^{207}Pb/^{204}Pb$	2σ	$^{208}Pb/^{204}Pb$	2σ	Model age (Ga)
Massive sulphide ore	HT-50	13.6485	±5	14.6137	±6	33.7288	±15	2.55
	HT-66	13.6343	±26	14.6251	±38	33.7386	±115	2.58
	HT-68	13.6209	±4	14.5946	±4	33.6418	±10	2.54
	HT-77	13.5829	±2	14.5211	±2	33.4219	±6	2.55
	HT-85	13.5935	±2	14.5199	±3	33.4272	±8	2.45
	HT-216	13.6096	±3	14.5718	±4	33.5719	±9	2.51
Ore mylonite	HT-5	14.2940	±3	14.7079	±3	34.2285	±10	1.98
	HT-9	13.5840	±2	14.5249	±3	33.4324	±9	2.45
	HT-16	14.0505	±2	14.6174	±3	34.1400	±9	2.07
	HT-90	13.7801	±5	14.5902	±7	33.7041	±22	2.34
	HT-91	13.5803	±3	14.5106	±3	33.3894	±8	2.43
	HT-228	13.7531	±2	14.5507	±3	33.6484	±7	2.29
Wallrock gneiss	HT-256	23.8400	±13	16.3562	±10	45.2352	±26	
	HT-260	27.8815	±8	17.1115	±5	47.2304	±15	
	HT-261	20.4260	±4	15.8199	±4	36.8798	±8	

Location of ore samples as in Table 1 except HT-228 from Stope 30 of Level-707 m. HT-256, HT-260 and HT-261 were collected on the surface. HT-256, anthophyllite–garnet gneiss; HT-260, biotite gneiss; HT-261, biotite–amphibole gneiss.

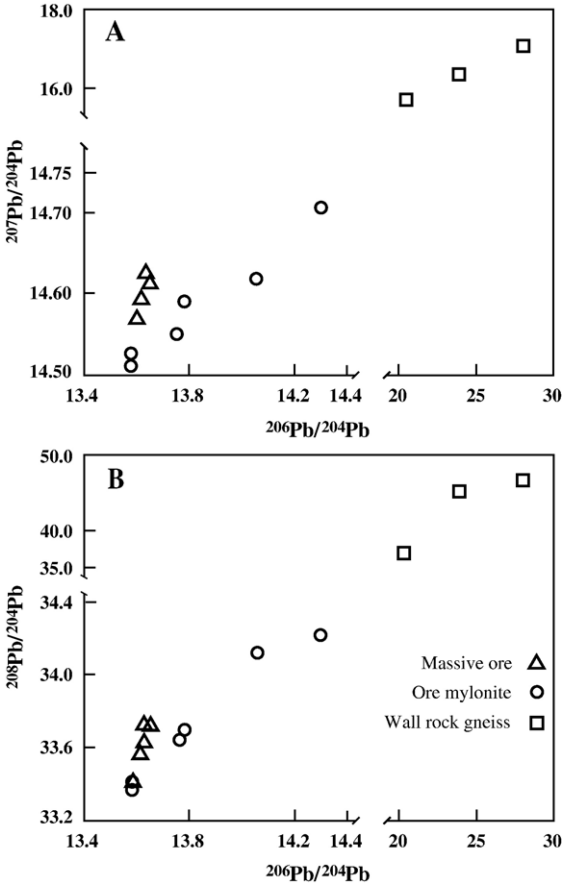

Fig. 11. Plots of lead isotope compositions of the massive ores, ore mylonites and wall rock gneisses from the Hongtoushan deposit.

dispersion. Such a distribution is likely to indicate that the lead in the massive ores came from two sources without significant differences in isotope compositions and mixed in various proportions. In contrast, lead isotope compositions of the ore mylonites are much wider in range, i.e., $^{206}Pb/^{204}Pb$=13.58 to 14.29, $^{207}Pb/^{204}Pb$=14.51 to 14.71, $^{208}Pb/^{204}Pb$=33.39 to 34.23. Plots of the data (Fig. 11) are generally scattered above, and to the right of those for the massive ores; lowest isotope ratios of both ore types are almost identical. More interestingly, wall rock gneiss samples of the Hongtoushan deposit are characterised by highly radiogenic lead, i.e., $^{206}Pb/^{204}Pb$=20.4260 to 27.8815, $^{207}Pb/^{204}Pb$=15.8199 to 17.1115, and $^{208}Pb/^{204}Pb$= 36.8798 to 47.2304, and plot approximately on the far extension of the ore mylonite trend on Fig. 11. These features may imply that the least radiogenic composition of the massive ores is closer to the lead originally accumulated during Archaean submarine exhalation. The most radiogenic leads of these two ore types suggest that the lead of the massive ores was overprinted by metamorphic fluids, and that minor but variable proportions of lead from the wall rocks were involved during formation of the ore mylonites. Since the massive sulphide ores have fairly low concentrations of both total lead and radiogenic lead, isotope compositions of the ore mylonites could be conspicuously modified by addition of even a minor amount of wall-rock-derived radiogenic lead. Similar Pb-isotope contamination from the wall rocks was reported by Chen (1994) for the ores in the Jiapigou gold deposit, which is about 70 km northeast of the Hongtoushan deposit.

Lead isotope ages calculated for the massive sulphide ores on the basis of the two-stage model developed by Stacey and Kramers (1975) vary in a narrow range from 2.58 to 2.45 Ga. This range is younger than the ages of formation (>3.0 Ga) and metamorphism (3.0–2.8 Ga) of the host strata given above, and could have been caused by addition of externally derived radiogenic Pb to these ores. Ages of the ore mylonites (2.45 to 1.98 Ga) are a little younger than the massive ores, indicating further incorporation of radiogenic Pb. The very high radiogenic lead of the wall rock gneisses indicates that the lead has resided in rock systems having high U/Pb and Th/Pb ratios and is not suitable for model age calculations (Faure, 1986).

8. Discussion on ore textures and metal enrichment in the oreshoots

8.1. Metamorphism of massive sulphide ores

Orebodies of the Hongtoushan deposit occur in the volcanic-sedimentary “rhythmic member” in the upper portion of the Hongtoushan Formation, and generally in parallel to the foliation of the wall rock gneisses. Banded ores also occur in the main orebodies, although massive sulphides dominate. The ores show no direct spatial relationship with known intrusive bodies in the mining area. These macroscopic features suggest that this deposit was initially formed on the seafloor by submarine exhalation in the Archaean (3.0 to 2.8 Ga), and then was intensely deformed and metamorphosed. Existence of sillimanite in the rocks suggests metamorphic temperatures >500 °C (Hietanenldsa, 1967; Richardson et al., 1969; Holdaway, 1971). Common occurrence of lath-like cubanite indicates a peak temperature higher than 557 °C (Cabri, 1973; Cabri et al., 1973). These data are consistent with the temperatures (600 to 650 °C) estimated by Zhao and Cui (1987) on the basis of biotite–garnet geothermometry.

As in many highly deformed and metamorphosed massive sulphide deposits elsewhere (e.g., Vokes, 1969; Craig and Vokes, 1993; Marshall and Gilligan, 1993; Cook, 1996), sedimentary ore textures at Hongtoushan have hardly been preserved; present textures were largely formed during peak and post-peak metamorphism. Felsic mineral globules composed of quartz and feldspar are likely to represent annealing equilibrium of felsic components with sulphide minerals at peak temperatures. The globular texture of the quartz and plagioclase may indicate relatively higher interfacial tensions of these two minerals against sulphides (c.f. Spry, 1979). Differential volume contraction between the globules and the neighbouring minerals induced the formation of micro-dilational fissures along grain boundaries. Selvages of hydrous minerals surrounding the globules are likely to have been developed by fluid infiltration and reaction along these fissures during retrograde metamorphism. Inclusions of pyrite, pyrrhotite, chalcopyrite and sphalerite inside the globular quartz and plagioclase can be considered as evidence for the sedimentary origin of these minerals. Replacement relics of plagioclase, sillimanite and sulphides in the dark mineral globules probably indicate that the dark mineral globules were formed by retrograde replacement of the plagioclase globules. Aluminum for the garnet and gahnite might have been derived from the plagioclase precursor, whereas zinc for the gahnite was obtained via desulphidation of sphalerite as suggested for other deposits (Spry and Scott, 1986; Spry et al., 2000). Mineralogy of the dark mineral globules implies that substantial replacement took place under conditions of the upper greenschist facies.

The presence of pyrrhotite inclusions in felsic globules and in pyrite porphyroblasts, and the optically continuous pyrrhotite islands separated by sillimanite imply that pyrrhotite is a pre-metamorphic mineral. The absence of exsolution lamellae in the pyrrhotite suggests that metamorphic annealing and homogenisation of monoclinic exsolution lamella affected this originally sedimentary mineral (c.f. Gu and Vokes, 1996).

Porphyroblasts of pyrite have inclusions of biotite, felsic mineral and dark mineral globules, and other sulphides, indicating that these porphyroblasts were formed during retrograde processes. Sulphur for the porphyroblasts might have derived partially from pyrrhotite since temperature decrease down to 305 or 254 °C (Arnold, 1967; Kissin and Scott, 1982) may cause sulphur exsolution from pyrrhotite, resulting in porphyroblastic growth of pyrite (Arnold, 1962; Yund and Hall, 1970; Craig and Vokes, 1993). However, pyrrhotite exsolution is far from enough to provide sulphur for all these porphyroblasts since the amount of pyrite often exceeds 10 vol.% in the ores. Experiments have proven that the sulphur content of hexagonal pyrrhotite in equilibrium with pyrite at 743 °C is below 55.1 at.% (Arnold, 1962), and that the minimum sulphide content of natural pyrrhotite is 52 at.% (Carpenter and Desborough, 1964). Therefore, exsolution can only produce sulphur no more than 3.1 at.% of the accompanying pyrrhotite. It follows that the ores at Hongtoushan may also contain a certain amount of sedimentary pyrite, which recrystallised in the course of prograde metamorphism and was overgrown during retrogression. Furthermore, equigranular pyritohedral pyrite amounting to more than 50 vol.% in some zinc ores might be essentially sedimentary in origin and had been subjected to prograde recrystallisation. Nevertheless, it is hard to determine whether a discrete pyrite porphyroblast was formed by prograde recrystallisation of sedimentary pyrite or by retrograde growth involving exsolved sulphur.

Straight crystal boundaries of cubic pyrite porphyroblasts against pyrrhotite, chalcopyrite and sphalerite depend on their stronger growth force than other sulphides (Craig and Vokes, 1993), whereas ragged boundaries against either the felsic mineral or dark mineral globules might indicate that the globules impeded growth of the pyrite. McClay and Ellis (1983) discussed the influence of matrix minerals on pyrite growth in more detail.

Magnetite in intergrowths with pyrrhotite and pyrite has been widely reported in metamorphosed massive sulphide ores (e.g., Gu et al., 1997; Alirezaei and Cameron, 2002). Such textures are likely to indicate that replacement reactions took place close to the magnetite–sulphide phase boundaries in a sulphide-buffered system, and that sulphur released by these reactions was limited in mobility in these Fe-rich systems. In the case of the Hongtoushan deposit, the magnetite–sulphide intergrowths replaced all the sulphide minerals including pyrite porphyroblasts, and their distribution does not seem to be fissure-controlled, but typically forms rings surrounding cores of anhydrite or carbonate. It follows that these intergrowths were probably formed during peak metamorphism. Volume contraction accompanying sulphide–magnetite conversion due to molar volume reduction (Seward and Barnes, 1997) might have created pores, which were filled later by anhydrite and carbonate.

The lack of chalcopyrite in sphalerite and monoclinic exsolution lamellae in pyrrhotite could be accounted for in terms of metamorphic annealing and homogenisation of the sphalerite and pyrrhotite grains (Craig, 1983, 1990; Eldridge et al., 1988; Gu and Vokes, 1996).

8.2. Metamorphic remobilisation

Intensive metamorphic remobilisation, both mechanical and chemical, occurred in the Hongtoushan deposit at scales ranging from the deposit to exposure and microscopic. Mechanical remobilisation accompanying deformation has modified the distribution of the ores. Transposition created the Y-shaped configuration of the main orebodies. Intense plastic flow moved the ores toward the vertical hinge of the deposit-scale synformal fold, resulting in the "ore pillar" with maximum width up to 40 m. Piercement cusps represent mining-surface-scale mechanical remobilisation. Microscopically, mechanical remobilisation is typified by chalcopyrite squeezed into pyrite cracks. These records of mechanical remobilisation were essentially written at elevated temperatures and pressures, particularly during prograde metamorphism.

Chemical remobilisation resulting from fluid flow is more important to redistribution of ore components throughout the deposit. Numerous unmetamorphosed sulphide-bearing quartz veins, which represent channellised fluid flow (c.f., Oliver, 1996), are widely seen cutting the Hongtoushan orebodies. The similarity of most of the veins to the massive ores in sulphide mineralogy, and the rare occurrence of sulphide-bearing veins outside the orebodies imply that sulphides in these veins were largely remobilised from the surrounding massive ores. In contrast to the high Zn/Pb ratio of the massive sulphide ores, however, the Zn-poor and Pb-rich nature of a vein may indicate that the lead for this vein came from a source outside the deposit. In addition to the veins, miscellaneous microscopic metasomatic textures produced by pervasive fluid flow (c.f., Oliver, 1996) have also been observed throughout the massive sulphide ores in the deposit.

Ore textures recorded both the starting- and ending-points of the remobilisation process. Starting-point textures for remobilisation of Cu and Zn are typically represented by chalcopyrite and sphalerite replaced by biotite and actinolite, and in places, by chalcopyrite replacement by symplectites of magnetite and pyrrhotite with or without pyrite. Ending-point textures for remobilisation of Cu and Zn are typically represented by chalcopyrite and sphalerite infillings along pyrite cleavages and by chalcopyrite overgrowths on the pyrite substrate. Chalcopyrite filling fractures with matching walls that are connected to chalcopyrite aggregates outside the veined pyrite could have been emplaced by solid-state remobilisation or plastic inflowing. The opening of these fractures may be due partly to the mechanical wedging of the invading chalcopyrite. However, in cases where chalcopyrite-filled fractures show corroded and hence non-matching walls, and where no chalcopyrite is present in the immediate vicinity of the veined pyrite, solid-state invasion is not a plausible explanation, and a mechanism involving fluid-state remobilisation can be considered (Marshall and Gilligan, 1987; Craig and Vokes, 1993). As a remobilisation product, cleavage-filling chalcopyrite in biotite was also reported by Cook et al. (1994) from the massive sulphide ores in the Matchless deposit, Namibia. Chalcopyrite disease of sphalerite represents both the remobilisation starting-point of Zn and the remobilisation ending-point of Cu. Selvages of hydrous minerals surrounding quartz globules and intensive replacement of plagioclase globules with resultant dark mineral globules prove that components for these gangues have also undergone extensive remobilisation. At the same time, radiogenic lead from outside the orebodies made the two-stage model ages of the ores younger than the formation age of the deposit.

All the products of chemical remobilisation in the Houngtoushan deposit lack deformation and metamorphic textures, implying that these products were formed during retrograde metamorphism. By contrast, records of pre-peak chemical remobilisation are rarely preserved in this deposit. These facts are likely to indicate that the majority of dissolved components in prograde fluids have been transported away down the temperature and pressure gradients to surrounding areas by either pervasive or channellised flows (Wood and Walther, 1986; Oliver, 1996, 2001; Marshall and Gilligan, 1993; Chen et al., 2003). Even if a certain amount of metals were initially unloaded inside the orebodies, they would have undergone reworking and further remobilisation in response to increasing temperature and pressure. However, at lowered temperatures of the post-peak stage, mechanical remobilisation is no longer important (Marshall and Gilligan, 1987, 1993), but fluid-state remobilisation is still active due to volume contraction and fracturing of the rocks and ores, resulting in redistribution of ore components and exchange of materials between orebodies and surrounding wallrocks (Chen et al., 2003). Furthermore, products of retrograde remobilisation are relatively stable against later events, and thus could be well preserved.

8.3. Formation mechanism of the oreshoots

Conspicuous foliations and highly reduced grain sizes indicate that the oreshoots of the Hongtoushan deposit are actually Cu- and Au-enriched ore mylonites. The existence of slip lines in the pyrite implies that

ductile shearing to form the ore mylonite took place at temperatures higher than 450 °C (Cox et al., 1981). The presence of annealing textures in pyrrhotite and the corresponding absence in pyrite suggest that formation and later annealing of the ore mylonite took place over the temperature range from 550 to 450 °C (Cox et al., 1981; Marshall and Gilligan, 1987), which is significantly lower than that for peak metamorphism of the deposit (600 to 650 °C). Combined with the fact that the oreshoots occur only in discrete zones, that hydrothermal alteration is characterised by amphiboles, epidote and albite, and that deformed minerals are less strongly annealed than in the massive ores, such a temperature range suggests that these ore mylonites and the derivative oreshoots were formed during retrograde metamorphism at upper-greenschist-facies. Under such conditions, micas, quartz, pyrrhotite, chalcopyrite and sphalerite are sufficiently ductile (Clark and Kelly, 1973; Simpson, 1985; Cox, 1987; Shu and Sun, 1996; Belkabir et al., 1998), but plagioclase, hornblende and pyrite remain brittle (McClay and Ellis, 1983; Belkabir et al., 1998; Ingles et al., 1999).

Previous authors (Q.S. Zhang et al., 1984; Liu et al., 1994) claimed that the oreshoots at Hongtoushan were formed by mechanical remobilisation, whereas the high enrichment of Cu, Au and Ag in the mylonitic ores was induced by differential plastic flow of the various minerals. They explained that Cu, Au and Ag minerals are more plastic than pyrite and gangue minerals, and thus have been squeezed preferentially into the space hosting the ore mylonites. However, not all the oreshoots are dominated by incompetent minerals. In some oreshoots, the competent mineral, pyrite, can exceed 50 vol.%, and therefore differential plastic flow is not a convincing mechanism. On the contrary, pressure solution of pyrite, fluid precipitation textures and externally derived lead isotope signatures suggest that the oreshoots were originally ore mylonite zones, which have been overprinted by late-stage fluids.

Various mechanisms for gold enrichment in ductile shear zones have been discussed in the literature (Eisenlohr et al., 1989; Mikucki, 1998; Chen and Fu, 1992; Chen, 1998; Groves et al., 2003). In the special case of ore mylonites of the Hongtoushan deposit, several mechanisms should be emphasised: (1) It has been proved by previous research that pressure solution is an important mechanism of ductile flow during shearing (Gu and McClay, 1992; Cook et al., 1993). Quartz, which is a dominant gangue of the massive sulphide ores, is more pressure-sensitive than common sulphide and silicate minerals (McClay, 1983a; Sun et al., 1984; Gu and McClay, 1992; Wu, 1998). Shearing of the ores will cause preferential dissolution and leaching of this mineral, resulting in relative enrichment of metals in the ore mylonites. (2) Enhanced porosity and permeability of the shear zones facilitate fluid percolation (e.g., Boulter, 1987; Chen, 1998; Bursnall, 1989). In particular, pore spaces formed by fragments of abundant and brittle pyrite can be well interconnected, and thus cause focusing of fluids (Oliver, 1996, 2001; Cartwright and Oliver, 2002), and provide loci for metal deposition. (3) Fragmentation, ductile deformation, recrystallisation and resultant grain-size reduction increase surface free energy of sulphide minerals and thus raise their reaction and overgrowth rates. Experiments performed by Gu et al. (2004, 2005) proved that tectonically crushed pyrite is a preferential substrate for chalcopyrite precipitation. Apart from Cu, Au adsorption onto the surface of sulphide minerals has already been considered as an important role in the precipitation of gold from hydrothermal fluids (e.g., Ramdohr, 1969; Seward, 1984; Bao, 1993; Genkin et al., 1998) and has been verified by a variety of experiments (Hyland and Bancroft, 1989; Schoonen et al., 1992; Maddox et al., 1998; Widler and Seward, 2002). Zhang et al. (1996) have shown experimentally that pyrite will become a stronger adsorbent for gold when it is more intensely crushed.

It has already been noted that chalcopyrite fills cracks and overgrows on pyrite grains more commonly than sphalerite in massive sulphide ores (Vokes, 1971). This is also the case in both the massive sulphide ores and ore mylonites at Hongtoushan. Furthermore, Cu has a much higher enrichment coefficient than Zn in the ore mylonites. One explanation for such phenomena is the higher metamorphic mobility of chalcopyrite than sphalerite (c.f. Vokes, 1971; Marshall and Gilligan, 1987; Gilligan and Marshall, 1987; Vokes and Craig, 1993). This is supported by the experimental results of Gu et al. (2005). However, the zoning from pyrite through chalcopyrite to sphalerite in the gneiss immediately adjacent to an oreshoot (Fig. 9E) proves that Zn is also a major component in the remobilising fluids. Such zoning is consistent with the fact that sphalerite has higher solubility in pyrite-buffered solutions than chalcopyrite in a wide range of temperatures (Large, 1992). Therefore, it is more likely that preferential precipitation of chalcopyrite is largely due to a solubility decrease of this mineral with temperature. In addition, pyrite seems to be a more favoured substrate for chalcopyrite growth than for sphalerite.

Although there is no clear distinction between possible metal sources for the oreshoots, the localised distribution of the oreshoots inside the massive sulphide

layers and similarity between the mylonitic and massive ores in metal varieties and lead isotope ages suggest that Cu, Au and Ag of the fluids that overprinted the ore mylonites were derived mainly from the nearby massive sulphide ores by internal remobilisation (Marshall and Gilligan, 1987, 1993). However, Pb isotope compositions of the ore mylonites also suggest that an external source, such as the metamorphic host rocks, has also contributed to the metal budget. Slightly younger Pb isotope two-stage model ages of the ore mylonite compared to the massive ores point to the incorporation of externally derived radiogenic lead.

The massive sulphide ores of the Hongtoushan deposit consist of a significant amount of incompetent sulphides such as pyrrhotite and chalcopyrite. These minerals are plastic enough to initiate ductile shearing even at temperatures below 300 °C (Clark and Kelly, 1973; Marshall and Gilligan, 1987). In the meantime, cataclasis and grain-size reduction of brittle minerals, such as the large pyrite porphyroblasts, could have facilitated grain boundary sliding and hence ductile shearing (Liu, 1988; Kerrich, 1989). Localised distribution of the ore mylonites could be accounted for by local nucleation of ductile shearing, while the varying size of the oreshoots seems to represent different growth stages of the shear zones (c.f. Christiansen and Pollard, 1997; Ingles et al., 1999). The shear zones could have nucleated on either local fluid accumulations (Christiansen and Pollard, 1997), or pre-existing fractures (Segall and Simpson, 1986; Gibson, 1990; Tourigny and Tremblay, 1997). Growth and development of these zones, even in the latter case, would also have been promoted by fluids because fluid infiltration can significantly enhance softening of the rocks by hydraulic weakening (Griggs and Blacic, 1965; Kirby, 1984; Ingles et al., 1999; Shu et al., 1999), grain-boundary sliding (Stanton, 1972; Marshall and Gilligan, 1987; Cox, 1987), pressure solution (McClay, 1977; Gu and McClay, 1992; Cook et al., 1993), formation of hydrous alteration minerals (Bursnall, 1989; Xu, 1996; Engvik et al., 2001), and precipitation of ductile sulphides (e.g. chalcopyrite and pyrrhotite, Marshall et al., 2000). Reduced grain sizes during shearing in turn facilitated further fluid focusing and its reaction with deformed minerals (Oliver, 2001; Musumeci, 2002), resulting in chemically enhanced porosity and permeability of the rocks (Hobbs, 1987; Rumble, 1994; Marshall et al., 2000). Therefore, formation of the ore mylonites is a process that involves complicated feedback between deformation, fluid flow and chemical reaction. Remobilising fluids precipitated Cu, Au and Ag in the ore mylonites until the pore spaces were ultimately sealed. The fact that overprinting metals on the ore mylonites came not only from the adjacent massive sulphide ores but also from metamorphic rocks surrounding the deposit indicates that even small-scale ductile shear zones are sufficiently open systems that are able to accept fluids for hydrothermal mineralisations.

9. Concluding remarks

The ores of the Hongtoushan Archaean volcanic-hosted massive sulphide deposit were originally domi-

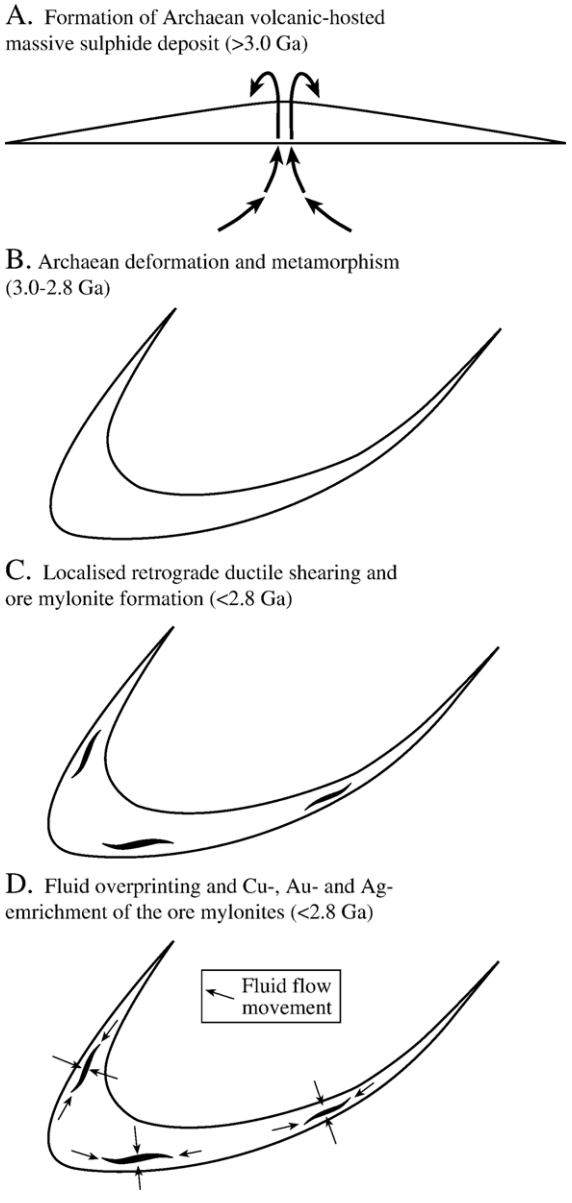

Fig. 12. Sequence of events that formed the Cu–Au–Ag-enriched oreshoots in massive sulphide orebodies at Hongtoushan.

nated by pyrrhotite, pyrite, sphalerite and chalcopyrite. Sedimentary ore textures were almost entirely obliterated by post-ore recrystallisation during deformation and upper-amphibolite-facies metamorphism. Present textures were formed substantially during peak and post-peak metamorphism. The disappearance of monoclinic exsolution lamellae in hexagonal pyrrhotite and chalcopyrite disease in sphalerite were caused by metamorphic homogenisation of the host pyrrhotite and sphalerite. Porphyroblasts of pyrite were formed partially by recrystallisation of sedimentary pyrite and partially by exsolved sulphur from pyrrhotite on cooling.

Intensive remobilisation occurred in the Hongtoushan deposit at various scales. Mechanical remobilisation took place accompanying prograde metamorphism and significantly modified the shapes and configuration of the orebodies. In contrast, the presently preserved records for chemical remobilisation were largely written at the retrograde stage and were represented by various replacement and fluid-precipitation textures in the ores as well as numerous undeformed sulphide-bearing veins.

In some localities, the massive ores were sheared at a temperature range of 550 to 450 °C in association with retrograde metamorphism, resulting in more than 30 ore mylonite zones. In these zones, pyrite is dominated by brittle deformation, although submicroscopic plastic deformation represented by slip lines also occurred. By contrast, pyrrhotite, chalcopyrite and sphalerite are dominated by plastic deformation. These ore mylonite zones were overprinted by late-stage fluids, resulting in oreshoots highly enriched in Cu, Au and Ag. Localised distribution of the oreshoots inside the massive sulphide orebodies, very small size of the recrystallised sulphide grains, and a gangue-mineral assemblage typical of the greenschist facies indicate that ductile-shearing and fluid overprinting took place at greenschist-facies retrograde metamorphism. The similarity of the ore mylonite to the massive ores in metal varieties and lead isotope ages suggest that Cu, Au and Ag of the overprinting fluids on the ore mylonites were derived mainly from the nearby massive sulphide ores by internal remobilisation. However, Pb isotope compositions of the ore mylonites also suggest that an external source, such as the metamorphic host rocks, also contributed to the metal budget. A summary of the sequence of events that formed the Hongtoushan deposit and the Cu–Au–Ag-enriched oreshoots is shown in Fig. 12.

Acknowledgements

This research was jointly supported by China Natural Science Foundation (Grant Nos. 40172034, 50234051, 40221301 and 40372092) and the International Exchange Programme of State Key Laboratory of Endogenic Metal Deposit Research (Nanjing University). Dr. Cao Jiahong is thanked for his participation in part of the work for this paper. The authors are grateful to the mining geologists Drs. Huang Mingran, Zhang Weichun, Lu Difu and Tan Liyong of Hongtoushan Mining Company and to Drs. Zhang Yonghong and Yang Tiejun of Fushun Institute of Geology and Ore Exploration for their help during underground and surface work. We are also indebted to Profs. Nigel Cook, Andreas Mueller and Steve Kesler, and an anonymous *Ore Geology Reviews* referee, whose careful reviews and kind comments have greatly improved the readability of this paper.

References

Alirezaei, S., Cameron, E.M., 2002. Mass balance during gabbro–amphibolite transition, Bamble Sector, Norway: implications for petrogenesis and tectonic setting of the gabbros. Lithos 60, 21–45.

Arnold, R.G., 1962. Equilibrium relations between pyrrhotite and pyrite from 325 °C to 743 °C. Economic Geology 57, 72–90.

Arnold, R.G., 1967. Range in composition and structure of 82 natural terrestrial pyrrhotites. Canadian Mineralogist 9, 31–50.

Bao, Z.X., 1993. Gold-bearing features of pyrite, arsenopyrite and stibnite in gold deposits of the Jiangnan paleo-island arc. Gold Science & Technology 1 (3), 40–47 (in Chinese).

Barton Jr., P.B., 1978. Some ore textures involving sphalerite from the Furutobe mine, Akita Prefecture, Japan. Mining Geology 28, 293–300.

Belkabir, A., Hubert, C., Hoy, L., 1998. Fluid–rock reactions and resulting change in rheological behavior of a composite granitoid: the Archaean Mooshla stock, Canada. Canadian Journal of Earth Sciences 35, 131–146.

Boulter, C.A., 1987. The Golden Mile, Kalgoorlie: a giant gold deposit localised in ductile shear zone by structurally induced infiltration of an auriferous metamorphic fluid. Economic Geology 82, 1661–1678.

Bursnall, J.T., 1989. Introduction: review of mechanical principles, deformation mechanisms and shear zone rocks. In: Bursnall, J.T. (Ed.), Mineralisation and Shear Zones, Geological Association of Canada Short Course Notes, vol. 6, pp. 1–28.

Cabri, L.J., 1973. New data on phase relation in the Cu–Fe–S system. Economic Geology 68, 443–454.

Cabri, L.J., Szymanski, J.T., Stewart, J.M., 1973. On the transformation of cubanite. Canadian Mineralogist 12, 33–38.

Carpenter, R.H., Desborough, B.A., 1964. Range in solid solution and structure of naturally occurring troilite and pyrrhotite. American Mineralogist 49, 1350–1365.

Cartwright, I., Oliver, N.H.S., 2002. Metamorphic fluids and their relationship to the formation of metamorphosed and metamorphogenic ore deposits. In: Spry, P.G., Marshall, B., Vokes, F.M. (Eds.), Metamorphosed and Metamorphogenic Ore Deposits, Reviews in Economic Geology, vol. 11, pp. 81–96.

Chen, P.J., 1989. Age and framework of horizontal displacement of the Tan–Lu fault. Chinese Science Bulletin 34, 482–487.

Chen, Y.J., 1994. The gold deposits in greenstone belts, China. In: The Gold Office of the Chinese Academy of Sciences (Ed.),

Current Progresses in the Study of Gold Deposits, China. Seismological Press, Beijing, pp. 4–29 (in Chinese).
Chen, Y.J., 1998. Fluidisation model for continental collision in special reference to study ore-forming fluid of gold deposits in the eastern Qinling Mountains, China. Progress in Natural Science 8 (4), 385–393.
Chen, Y.J., Fu, S.G., 1992. Gold Minerlisation in West Henan. Chinese Seismological Press, Beijing. 234 pp. (in Chinese).
Chen, Y.J., Yang, J.Q., Deng, J., Ji, H.Z., Fu, S.G., Zhou, X.P., Lin, Q., 1996. Turning point in the evolution history of the Earth: 2300 Ma. Geology and Geochemistry 3, 106–124 (in Chinese).
Chen, Y.J., Guo, G.J., Li, X., 1998. Metallogenic geodynamic background of gold deposits in granite–greenstone terrains of North China craton. Science in China (series D) 41 (2), 113–120.
Chen, B., Jahn, B., Wilde, S., Xu, B., 2000. Two contrasting Paleozoic magmatic belts in northern Inner Mongolia, China: petrogenesis and tectonic implications. Tectonophysics 328, 157–182.
Chen, Y.J., Sui, Y.H., Pirajno, F., 2003. Exclusive evidence for CMF model and a case of orogenic silver deposits: isotope geochemistry of the Tieluping silver deposit, east Qinling orogen. Acta Petrologica Sinica 19, 551–568 (in Chinese with English abstract).
Christiansen, P.P., Pollard, D.D., 1997. Nucleation, growth and structural development of mylonitic shear zones in granitic rocks. Journal of Structural Geology 19, 1159–1172.
Clark, B.R., Kelly, W., 1973. Sulfide deformation studies: I. Experimental deformation of pyrrhotite and sphalerite to 2000 bars and 500 °C. Economic Geology 68, 332–352.
Cook, N.J., 1996. Mineralogy of the sulphide deposits at Sulitjelma, northern Norway. Ore Geology Reviews 11, 303–338.
Cook, N.J., Halls, C., Boyle, A.P., 1993. Deformation and metamorphism of massive sulphides at Sulitjelma, Norway. Mineralogical Magazine 57, 67–81.
Cook, N.J., Klemd, R., Okrusch, M., 1994. Sulphide mineralogy, metamorphism and deformation in the Matchless massive sulphide deposit, Namibia. Mineralium Deposita 29, 1–15.
Cox, S.F., 1987. Flow mechanisms in sulphide minerals. Ore Geology Reviews 2, 133–171.
Cox, S.F., Etheridge, M.A., Hobbs, B.E., 1981. The experimental ductile deformation of polycrystalline and single crystal pyrite. Economic Geology 76, 2105–2117.
Craig, J.R., 1983. Metamorphic features in Applachian massive sulphides. Mineralogical Magazine 47, 515–525.
Craig, J.R., 1990. Textures of the ore minerals. In: Jambor, J.L., Vaughan, D.J. (Eds.), Advanced Microscopic Studies of Ore Minerals, Mineralogical Association of Canada Short Course Handbook, vol. 17, pp. 213–262.
Craig, J.R., Vaughan, D.J., 1981. Ore Microscopy and Ore Petrography. John Wiley, New York. 406 pp.
Craig, J.R., Vokes, F.M., 1993. The metamorphism of pyrite and pyritic ores: an overview. Mineralogical Magazine 57, 3–18.
Deng, G.Q., 1994. Base metal deposit of the Liaodong–Jinan terrane. In: Rui, Z.Y., Shi, L.D., Fang, R.H. (Eds.), Geology of Nonferrous Metallic Deposits in Northern Margin of the North China Landmass and Adjacent areas. Geological Publishing House, Beijing, pp. 25–52 (in Chinese with English abstract).
Duckworth, R.C., Rickard, D., 1993. Sulphide mylonites from the Renström VMS deposit, Northern Sweden. Mineralogical Magazine 57, 83–92.
Eisenlohr, B.N., Groves, D.I., Partington, G.A., 1989. Crustal-scale shear zones and their significance to Archaean gold mineralisation in Western Australia. Mineralium Deposita 24, 1–8.
Eldridge, C.S., Barton, P.B., Ohmoto, H., 1983. Mineral textures and their bearing on formation of the Kuroko orebodies. Economic Geology Monographs 5, 241–281.
Eldridge, C.S., Bourcier, W.L., Ohmoto, H., Barnes, H.L., 1988. Hydrothermal inoculation and incubation of the chalcopyrite disease in sphalerite. Economic Geology 82, 978–989.
Engvik, A.K., Austrheim, H., Erambert, M., 2001. Interaction between fluid flow, fracturing and mineral growth during eclogitization, an example from the Sunnfjord area, Western Gneiss Region, Norway. Lithos 57, 111–141.
Faure, G., 1986. Principles of Isotope Geology, second edition. John Wiley, New York. 589 pp.
Fitches, W.R., Fletcher, C.J.N., Xu, J.W., 1991. Geotectonic relationships between cratonic blocks in east China and Korea. Journal of Southeast Asian Earth Sciences 6, 185–199.
Fletcher, C.J.N., Fitches, W.R., Rundle, C.C., Evans, J.A., 1995. Geological and isotopic Constraints on the timing of movement in the Tan–Lu Fault Zone, northeastern China. Journal of Southeast Asian Earth Sciences 11, 15–22.
Genkin, A.D., Bortnikov, N.S., Cabri, L.J., Wagner, F.E., Stanley, C.J., Safonov, Y.G., McMahon, G., Friedl, J., Kerzin, A.L., Gamyanin, G.N., 1998. A multidisciplinary study of invisible gold in arsenopyrite from four mesothermal gold deposits in Siberia, Russian Federation. Economic Geology 93, 463–487.
Gibson, R.G., 1990. Nucleation and growth of retrograde shear zones: an example from the Needle Mountains, Colorado, USA. Journal of Structural Geology 12, 339–350.
Gilligan, L.B., Marshall, B., 1987. Textural evidence for remobilisation in metamorphic environment. Ore Geology Reviews 2, 205–229.
Griggs, D.T., Blacic, J.D., 1965. Quartz: anomalous weakening of synthetic crystals. Science 147, 292–295.
Grotenhuis, S.M., Trouw, R.A.J., Passchier, C.W., 2003. Evolution of mica fish in mylonitic rocks. Tectonophysics 372, 1–21.
Groves, D.I., Goldfarb, R.J., Robert, F., Hart, C.J.R., 2003. Gold deposits in metamorphic belts: overview of current understanding, outstanding problems, future research and exploration significance. Economic Geology 98, 1–29.
Gu, L.X., McClay, K.R., 1992. Pyrite deformation in stratiform lead–zinc deposits of the Canadian Cordillera. Mineralium Deposita 27, 169–181.
Gu, L.X., Vokes, F.M., 1996. Intergrowth of hexagonal and monoclinic pyrrhotites in some sulphide ores from Norway. Mineralogical Magazine 60, 304–316.
Gu, L.X., Zhang, W.L., Yin, L., 1997. Symplectite of pyrite and magnetite in the sulphide ore from Mashan, Anhui Province. Chinese Journal of Geochemistry 6 (4), 359–362.
Gu, L.X., Zhou, B., Zhang, W.L., 1998. Chalcopyrite intergrowths in sphalerite in the Meixian lead–zinc deposit, Fujian Province and their metallogenetic significance. Chinese Journal of Geochemistry 17 (4), 311–319.
Gu, L.X., Hu, S.X., Chu, Q., Yu, C.S., Xiao, X.J., 1999. Pre-collision granites and post-collision intrusive assemblage of the Kelameili–Harlik orogenic belt. Acta Geologica Sinica (English edition) 73, 316–329.
Gu, L.X., Xiao, X.J., Ni, P., Wu, C.Z., 2001. Pyrrhotite textures and their genetic implications in the Hongtoushan Massive sulphide deposit, Liaoning Province, China. Chinese Journal of Geochemistry 20 (3), 210–217.
Gu, L.X., Tang, X.Q., Wang, Z.J., Sun, Y., Wu, C.Z., Xiao, X.J., Ni, P., Wu, X.Y., 2004. Remobilisation experiment of chalcopyrite in

massive sulphide ore by NaCl solution at 362 °C and a differential stress. Lithos 73, 47 (suppl.).

Gu, L.X., Tang, X.Q., Wang, Z.J., Wu, C.Z., Lu, J.J., Ni, P., Wu, X., 2005. Sulphide remobilisation in NaCl solution at temperature of 362 °C under differential stress. Acta Petrologica Sinica 21, 1429–1434 (in Chinese with English abstract).

Hart, C.J.R., Goldfarb, R.J., Qiu, Y., Snee, L., Miller, L.D., Miller, M.L., 2002. Gold deposits of the northern margin of North China Craton: multiple late Paleozoic–Mesozoic mineralising events. Mineralium Deposita 37, 326–351.

Hietanenldsa, A., 1967. On the facies series in various types of metamorphism. Journal of Geology 75, 187–214.

Hobbs, B.E., 1987. Principles involved in mobilisation and remobilisation. Ore Geology Reviews 2, 37–45.

Holdaway, M.J., 1971. Stability of andalusite and the aluminosilicate phase diagram. American Journal of Science 271, 97–131.

Hong, D.W., Huang, H.Z., Xiao, Y.J., Xu, H.M., Jin, M.Y., 1995. Permian alkaline granites in central Inner Mongolia and their geodynamic significance. Acta Geologica Sinica 8, 27–39.

Hou, Z.Q., Deng, J., Sun, H.T., Song, S.H., 1999. Volcanogenic massive sulphide deposits in China: setting, feature and style. Exploration and Mining Geology 8, 149–175.

Hyland, J.M., Bancroft, G.M., 1989. An XPS study of gold deposition at low temperatures on sulphide minerals: reducing agents. Geochimica et Cosmochimica Acta 53, 367–372.

Ingles, J., Lamouroux, C., Soula, J.C., Guerrero, N., Debat, P., 1999. Nucleation of ductile shear zones in a granodiorite under greenschist facies conditions, Nèouvielle massif, Pyrenees, France. Journal of Structural Geology 21, 555–576.

Kerrich, R., 1989. Geodynamic setting and hydraulic regimes: shear zone hosted mesothermal gold deposits. In: Bursnall, J.T. (Ed.), Mineralisation and Shear Zones, Geological Association of Canada Short Course Notes, vol. 6, pp. 89–128.

Kirby, S.H., 1984. Chemical effects of water on rock deformation. Journal of Geophysical Research 89, 3991–3995.

Kissin, S.A., Scott, S.D., 1982. Phase relations involving pyrrhotite below 350 °C. Economic Geology 77, 1739–1754.

Khin Zaw, Large, R.R., Huston, D.L., 1997. Petrological and geochemical significance of a Devonian replacement zone in the Cambrian Rosebery massive sulphide deposit, western Tasmania. Canadian Mineralogist 35, 1325–1349.

Khin Zaw, Huston, D.L., Large, R.R., 1999. A chemical model for remobilisation of ore constituents during Devonian replacement process within Cambrian VHMS Rosebery deposit, western Tasmania. Economic Geology 94, 529–546.

Large, R.R., 1992. Australian volcanic-hosted massive sulphide deposits: features, styles, and genetic models. Economic Geology 87, 471–510.

Li, J.J., Shen, B.F., Li, S.B., Mao, D.B., 1995. The Geology and Gold Mineralisation of the Greenstone Belts in Qingyuan–Jiapigou Region, China. Tianjin Science and Technology Press, Tianjin. 132 pp.

Li, J.Y., Mo, S., He, Z., Sun, G., Chen, W., 2004. The timing of crustal sinistral strike-slip movement in the northern Great Khing'an ranges and its constraint on reconstruction of the crustal tectonic evolution of NE China and adjacent areas since the Mesozoic. Earth Science Frontiers 11 (3), 157–168.

Liou, J.G., Wang, X., Coleman, R.G., Zhang, Z.M., Narytana, S., 1989. Blueschists in major suture zones of China. Tectonics 8, 609–619.

Liu, R.X., 1988. Geological Structures under the Microscope. Publishing House of Peking University, Beijing. 235 pp (in Chinese).

Liu, L.D., Zhu, Y.Z., Dai, S.B., 1994. Relationships between gold deposits and ductile shear zones and overprint structures. In: Zhang, Y.X., Liu, L.D. (Eds.), Precambrian Ore Deposits and Tectonics in China. Seismological Publishing House, Beijing, pp. 39–77 (in Chinese).

Lu, W.J., 1994. Geology and Genesis of the Hongtoushan Copper–zinc deposit. Geology of Liaonin Nonferrous Metals (1), 1–11 (in Chinese).

Lydon, J.W., Paakki, J.J., Anderson, H.E., Reardon, N.C., 2000. An overview of the geology and geochemistry of the Sullivan deposit. In: Lydon, J.W., Höy, T.H., Slack, J.F., Knapp, M.E. (Eds.), The Geological Environment of the Sullivan Deposit, British Columbia, Geological Association of Canada, Mineral Deposits Division, Special Publication, vol. 1, pp. 505–522.

Maddox, L.M., Bancroft, G.M., Scaini, M.J., Lorimer, J.W., 1998. Invisible gold: comparison of Au deposition on pyrite and arsenopyrite. American Mineralogist 83, 240–1245.

Marshall, B., Gilligan, L.B., 1987. An introduction to remobilisation: information from ore-body geometry and experimental considerations. Ore Geology Reviews 2, 87–131.

Marshall, B., Gilligan, L.B., 1989. Durchbewegung structures, piercement cusps, and piercement veins in massive sulphide deposits: formation and interpretation. Economic Geology 84, 2311–2319.

Marshall, B., Gilligan, L.B., 1993. Remobilisation, syn-tectonic processes and massive sulphide deposits. Ore Geology Reviews 8, 39–64.

Marshall, B., Vokes, F.M., Larocque, A.C.L., 2000. Regional metamorphic remobilisation: upgrading and formation of ore deposits. In: Spry, P.G., Marshall, B., Vokes, F.M. (Eds.), Metamorphosed and Metamorphogenic Ore Deposits, Reviews in Economic Geology, vol. 11, pp. 19–38.

McClay, K.R., 1977. Pressure solution and Coble creep in rocks and minerals: a review. Journal of the Geological Society of London 134, 57–70.

McClay, K.R., 1983a. Deformation of stratiform lead–zinc deposits. In: Sangster, D.F. (Ed.), Sediment-Hosted stratiform Lead–Zinc Deposits, Short Course Handbook, Mineral Association of Canada, vol. 8, pp. 283–309.

McClay, K.R., 1983b. Structural evolution of the Sullivan Fe–Pb–Zn–Ag orebody, Kimberley, British Columbia, Canada. Economic Geology 78, 1398–1424.

McClay, K.R., Ellis, P.G., 1983. Deformation and crystallisation of pyrite. Mineralogical Magazine 47, 527–538.

Mikucki, E.J., 1998. Hydrothermal transport and depositional process in Archaean lode-gold systems: a review. Ore Geology Reviews 13, 307–321.

Miyashiro, A., 1994. Metamorphic Petrology. University College London Press, London. 404 pp.

Musumeci, G., 2002. Sillimanite-bearing shear zones in syntectonic leucogranite: fluid assisted brittle ductile deformation under amphibolite facies conditions. Journal of Structural Geology 24, 1491–1505.

Oliver, N.H.S., 1996. Review and classification of structural controls on the fluid flow during regional metamorphism. Journal of Metamorphic Geology 14, 477–492.

Oliver, N.H.S., 2001. Linking of regional and local hydrothermal systems in the mid-crust by shearing and faulting. Tectonophysics 335, 147–161.

Paakki, J.J., Lydon, J.W, Del Bel Belluz, N., 1995. Durchbewegt sulphides, piercement structures, and gabbro dyke displacement in the vent complex of the Sullivan Pb–Zn deposit, British Co-

lumbia. Current Research - Geological Survey of Canada 1995-A, 81–90.
Ramdohr, P., 1969. The Ore Minerals and their Intergrowth. Pergamon Press, Oxford. 1174 pp.
Ren, J.S., 1996. The continental tectonics of China. Journal of Southeast Asian Earth Sciences 13, 197–204.
Richardson, S.W., Gilbert, M.C., Bell, P.M., 1969. Experimental determination of kynite–andalusite and andalusite–sillimanite equilibria; the aluminum silicate triple point. American Journal of Science 267, 259–272.
Robinson, P.T., Zhou, M., Hu, X., Reynolds, P., Bai, W.J., Yang, J., 1999. Geochemical constraints on the origin of the Hegenshan ophilite, Inner Mongolia, China. Journal of Asian Earth Sciences 17, 423–442.
Rumble III, D., 1994. Water circulation in metamorphism. Journal of Geophysical Research 99, 15499–15502.
Schoonen, M.A.A., Fisher, N.S., Wente, M., 1992. Gold sorption onto pyrite and goethite: a radiotracer study. Geochimca et Cosmochimica Acta 56, 1801–1814.
Segall, P., Simpson, C., 1986. Nucleation of ductile shear zones on dilatant fractures. Geology 14, 56–59.
Sengör, A.M.C., Natal'in, B.A., Burtman, V.S., 1993. Evolution of the Altaid tectonic collage and Paleozoic crustal growth in Eurasia. Nature 364, 299–307.
Seward, T.M., 1984. The transport and deposition of gold in hydrothermal systems. In: Foster, R.P. (Ed.), GOLD'82: The Geology, Geochemistry and Genesis of Gold Deposits. Balkema, Rotterdam, pp. 165–181.
Seward, T.M., Barnes, H.L., 1997. Metal transport by hydrothermal ore fluids. In: Barnes, H.L. (Ed.), Geochemistry of Hydrothermal Ore Deposits, 3rd edition. John Wiley, New York, pp. 435–486.
Shen, B.F, Lo, H., Han, G.G., Dai, X.Y., Jin, W.S., Hu, X.D., Li, S.B., Bi, S.Y., 1994a. Archaean Geology and Metallisation in Northern Liaoning Province and Southern Jilin Province. Geological Publishing House, Beijing. 255 pp. (in Chinese).
Shen, B.F., Peng, X.L., Luo, H., Jin, W.S., Hu, X.D., LI, S.B., Li, J.J., Chen, Y.H., 1994b. Archaean greenstone belts and related ore deposits in the North China Platform. In: Zhang, Y.X., Liu, L.D. (Eds.), Precambrian Ore Deposits and Tectonics in China. Seismological Publishing House, Beijing, pp. 1–38 (in Chinese).
Shu, L.S., Sun, Y., 1996. Simulating experiments for the deformation and microstructures of granites in the central part of the Jiangnan Belt, South China. Science in China (series D, English edition) 39 (1), 82–92.
Shu, L.S., Charvet, J., Guo, L.Z., Lu, H.F., Laurent-Charvet, S., 1999. A large-scale Palaeozoic dextral ductile strike-slip zone: the Aqqikkudug–Weiya zone along the Northern Margin of the Central Tianshan belt, Xinjiang, NW China. Acta Geologica Sinica (English edition) 73, 148–162.
Simpson, C., 1985. Deformation of granitic rock across the brittle–ductile transition. Journal of Structural Geology 7, 503–511.
Song, B., Nutman, A.P., Liu, D., Wu, J., 1996. 3800 to 2500 Ma crustal evolution in the Anshan area of Liaoning Province, northeastern China. Precambrian Research 78, 79–94.
Spry, A., 1979. Metamorphic Textures. Pergamon Press, Oxford. 350 pp.
Spry, P.G., Scott, S.D., 1986. The stability of zincian spinels in sulfide systems and their potential as exploration guides for metamorphosed massive sulphide deposits. Economic Geology 81, 1146–1163.
Spry, P.G., Peter, J.M., Slack, J.F., 2000. Meta-exhalites as exploration guides to ore. In: Spry, P.G., Marshall, B., Vokes, F.M. (Eds.), Metamorphosed and Metamorphogenic Ore Deposits, Reviews in Economic Geology, vol. 11, pp. 163–201.
Stacey, J.S., Kramers, J.D., 1975. Approximation of terrestrial lead isotope evolution by a two-stage model. Earth and Planetary Science Letters 26, 207–221.
Stanton, R.L., 1972. Ore Petrology. McGraw-Hill, New York. 713 pp.
Sun, H.T., 1992. A general review of volcanogenic massive sulphide deposit in China. Ore Geology Reviews 7, 43–71.
Sun, Y., Zhang, Q.L., Yang, S.F., 1984. On the evolution f pressure solution. Acta Mineralogica Sinica 1, 35–41 (in Chinese with English abstract).
Sun, Y., Xu, S.J., Lu, J.J., Lin, A.M., Liu, D.L., 1998. An Introduction to Tectonogeochemistry in Fault Zones. Science Press, Beijing. 246 pp. (in Chinese).
Tang, K.D., 1990. Tectonic development of Paleozoic foldbelts at the northern margin of the Sino-Korean craton. Tectonics 9, 249–260.
Tian, Z.Y., Han, P., Xu, K.D., 1992. The Mesozoic–Cenozoic East China rift system. Tectonophysics 208, 314–363.
Tiwary, A., Deb, M., Cook, N.J., 1998. Use of pyrite microfabric as a key to tectono-thermal evolution of massive sulphide deposits — an example from Deri, southern Rajasthan, India. Mineralogical Magazine 62, 197–212.
Tourigny, G., Tremblay, A., 1997. Origin and incremental evolution of brittle/ductile shear zones in granitic rocks: natural examples from the southern Abitibi Belt, Canada. Journal of Structural Geology 19, 15–27.
Vivallo, W., Rickard, D., 1990. Genesis of an Early Proterozoic zinc deposit in high-grade metamorphic terrane, Saxberget, Central Sweden. Economic Geology 85, 714–736.
Vokes, F.M., 1969. A review of the metamorphism of sulphide deposits. Earth-Science Reviews 5, 99–143.
Vokes, F.M., 1971. Some aspects of the regional metamorphic mobilization of pre-existing sulphide deposits. Mineralium Deposita 6, 122–129.
Vokes, F.M., 2000. Ores and metamorphism: introduction and historical perspectives. In: Spry, P.G., Marshall, B., Vokes, F.M. (Eds.), Metamorphosed and Metamorphogenic Ore Deposits, Reviews in Economic Geology, vol. 11, pp. 1–18.
Vokes, F.M., Craig, J.R., 1993. Post-recrystallisation mobilisation phenomena in metamorphosed stratabound sulphide ores. Mineralogical Magazine 57, 19–28.
Wang, Q., Liou, X.Y., 1986. Paleoplate tectonics between Cathaysia and Angaraland in Inner Mongolia of China. Tectonics 5, 1073–1088.
Wang, Q., Liu, X., 1991. Pre-Jurassic tectonic evolution between Cathaysia and Angaraland in Inner Mongolia of China. In: Ishii, K., Xueya, L., Ichikawa, K., Huang, B. (Eds.), Pre-Jurassic Geology of Inner Mongolia, China. China–Japan Cooperative Research Group, pp. 127–147.
Wang, S.S., Zhai, M.G., Hu, S.L., Sang, H.Q, Qiu, J., 1986. $^{40}Ar/^{39}Ar$ plateau age of the Shujigou tonalite at Qingyuan. Scientia Geologica Sinica 1, 97–99 (in Chinese).
Wang, S.S., Hu, S.L., Zhai, M.G., Sang, H.Q., Qiu, J., 1987. An application of the $^{40}Ar/^{39}Ar$ dating technique to the formation time of Qingyuan granite–greenstone terrain in NE China. Acta Petrologica Sinica 4, 55–62 (in Chinese).
Widler, A.M., Seward, T.M., 2002. The adsorption of gold(I) hydrosulphide complexes by iron sulphide surfaces. Geochimica et Cosmochimica Acta 66, 383–402.
Wood, B.J., Walther, J.V., 1986. Fluid flow during metamorphism and its implications for fluid–rock ratios. In: Walther, J.V., Wood, B.J.

(Eds.), Fluid–Rock Interactions during Metamorphism. Springer, New York, pp. 89–108.
Wu, X.Y., 1998. An Introduction to Tectonogeochemistry. Guizhou Science and Technology Press, Guiyang. 416 pp. (in Chinese).
Xu, X.C., 1996. Advances in the study of metamorphic fluids. Earth Sciences Frontiers 3, 200–206 (in Chinese).
Xu, Y.G., 2001. Thermo-Tectonic Destruction of the Archaean Lithospheric Keel Beneath the Sino-Korean Craton in China: Evidence, Timing and Mechanism. Physics and Chemistry of the Earth (series A) 26, 747–757.
Xu, B., Chen, B., 1997. The structure and evolution of a Middle-Paleozoic orogenic belt between the North China and Siberian Blocks, northern Inner Mongolia, China. Science in China (Series D) 27 (3), 227–232. (in Chinese with English abstract).
Xu, J.W., Zhu, G., 1994. Tectonic models of the Tan–Lu fault zone, eastern China. International Geology Review 36, 771–784.
Xu, J.W., Zhu, G., Tang, W.X., Cui, K.R., Lu, Q., 1987. Formation and evolution of the Tancheng–Lujiang wrench fault system: a major shear system to the northwest of the Pacific Ocean. Tectonophysics 134, 273–310.
Yang, Z.S., Yu, B.X., 1984. Poly-deformation of the Archaean greenstone belt in the Hongtoushan area, Northern Liaoning province. Bulletin of Changchun College of Geology (1), 20–35 (in Chinese).
Yang, Z.Y., Cheng, Y.Q., Wang, H.Z., 1986. The Geology of China. Clarendon Press, Oxford. 303 pp.
Yang, J.H., Wu, F.Y., Wilde, S.A., 2003. A review of the geodynamic setting of large-scale Late Mesozoic gold mineralisation in the North China Craton: an association with lithospheric thinning. Ore Geology Reviews 23, 125–152.
Yund, R.A., Hall, H.T., 1970. Kinetics and mechanism of pyrite exsolution from pyrrhotite. Journal of Petrology 11, 381–404.
Zhai, M.G., Liu, W.J., 2001. The formation and contribution of granulites to the evolution of the continental crust. Acta Petrologica Sinica 17 (1), 28–37 (in Chinese with English abstract).
Zhai, M.G., Liu, W.J., 2003. Paleoproterozoic tectonic history of the North China Craton: a review. Precambrian Research 122, 183–199.
Zhai, M.G., Yang, R.Y., Lu, W.J., Shao, J.P., 1984. Major and trace element geochemistry of the Archaean Qingyuan granite–greenstone terrane. Geological Review 30, 523–535 (in Chinese).
Zhang, Q.S., Li, S.Y., Liu, L.D., 1984. Geology and Metallogeny of the Early Precambrian in China. Jilin People's Publishing House, Changchun. 536 pp. (in Chinese).
Zhang, Z.M., Liou, J.R., Coleman, R.G., 1984. An outline of the plate tectonics of China. Geological Society of America Bulletin 95, 295–312.
Zhang, S.B., Wu, D.Q., Xie, X.D., 1996. An experimental study of adsorption of gold complexes by pyrite from different deposits. Geochimica 25 (1), 84–92 (in Chinese).
Zhao, S.X., 1981. Characteristics and possible seismological hazard of the Hunbei fault. Liaonin Geologic Information (2), 61–72 (in Chinese with English abstract).
Zhao, Y.X., Cui, W.Y., 1987. Mineralogy and *P–T* conditions of crystallisation of Archaean metamorphic complex from Qingyuan district, Liaoning Province. Journal of Changchun University of Earth Science, Special Issue of Metamorphic Geology, 191–204 (in Chinese).
Zhao, G.C., Wilde, S.A., Cawood, P.A., Sun, M., 2001. Archaean blocks and their boundaries in the North China Craton: lithological, geochemical, structural and *P–T* path constraints and tectonic evolution. Precambrian Research 107, 45–73.
Zhou, T.H., Goldfarb, R.J., Phillips, G.N., 2002. Tectonics and distribution of gold deposits in China — an overview. Mineralium Deposita 37, 249–282.
Zhu, G., Hou, M.J., Wang, Y.S., Liu, G.S., Niu, M.N., 2004. Thermal evolution of the Tanlu fault zone on the eastern margin of the Dabie Mountains and its tectonic implications. Acta Geologica Sinica (English edition) 4, 940–953.